# REPORT DOCUMENTATION PAGE

AFRL-SR-AR-TR-03-

0143

| 1. REPORT DATE (DD-MM-YYYY) | 2. REPORT DATE | 3. DATES COVERED (From - To) |
|---|---|---|
| 31-DEC-2002 | 12/31/02 | 2/15/00-12/31/02 |

| 4. TITLE AND SUBTITLE | 5a. CONTRACT NUMBER |
|---|---|
| Implementation of Microwave Active Nulling | F49620-00-C0016 |
| | 5b. GRANT NUMBER |
| | 5c. PROGRAM ELEMENT NUMBER |

| 6. AUTHOR(S) | 5d. PROJECT NUMBER |
|---|---|
| Hoton How, Carmine Vittoria | FO8671-0000636 2304/BX |
| | 5e. TASK NUMBER |
| | 5f. WORK UNIT NUMBER |

| 7. PERFORMING ORGANIZATION NAME(S) AND ADDRESS(ES) | 8. PERFORMING ORGANIZATION REPORT NUMBER |
|---|---|
| ElectroMagnetic Applications, Inc.<br>300 Commercial St., U805<br>Boston, MA 02105 | AFR - 1 |

| 9. SPONSORING/MONITORING AGENCY NAME(S) AND ADDRESS(ES) | 10. SPONSOR/MONITOR'S ACRONYM(S) |
|---|---|
| Air Force Office of Scientific Research<br>801 North Randolph St., Rm 732<br>Arlington, VA 22203-1977 | AFOSR CODE FA9550 A002 |
| | 11. SPONSORING/MONITORING AGENCY REPORT NUMBER |
| | Final Report |

**12. DISTRIBUTION AVAILABILITY STATEMENT**

AFOSR

**13. SUPPLEMENTARY NOTES**

None

**14. ABSTRACT**

We have fabricated a universal test equipment capable of measuring the phase and amplitude of the reflection wave from a coax-cable cavity resonator. Frequency-agile materials, such as ferroelectric and ferrite samples were included with the resonator so that the resonant frequency of the resonator can be tuned by applying either a bias electric voltage or a bias magnetic field. Sensitive electric and magnetic tuning have been obtained, and the measurement results compared nicely with calculations. In order to enhance the sensitivity of electronic tuning resonance mechanisms have been incorporated with the reflector performance, such as the structural resonance and the ferrimagnetic resonance.

**15. SUBJECT TERMS**

Active Nulling, Microwave Reflector, Phase Shifter

| 16. SECURITY CLASSIFICATION OF: | | | 17. LIMITATION OF ABSTRACT | 18. NUMBER OF PAGES | 19a. NAME OF RESPONSIBLE PERSON |
|---|---|---|---|---|---|
| a. REPORT | b. ABSTRACT | c. THIS PAGE | | | Anmarie Vittoria |
| U | U | U | UU | 75 | 19b. TELEPONE NUMBER (include area code)<br>(617)720-3968 |

20030513 087

# Implementation of Microwave Active Nulling

Hoton How and Carmine Vittoria
ElectroMagnetic Applications, Inc.
300 Commercial St., Suite 805, Boston, MA 02109
phone: (617)720-3968, fax: (617)720-3968
email: HHOW@YAHOO.COM, VITTORIA@NEU.EDU

Key Words: Active Nulling, Microwave Reflector, Phase Shifter

## BACKGROUND

Microwave and millimeter-wave (MMW) devices and systems are becoming increasingly important today for both defense and commercial applications. For example, in the collision avoidance industries, low-profile antennas are needed providing electronically steerable radiations to detect and identify obstacles and intrusions in front of a moving vehicle. Upon navigation the receiver antennas need to follow and trace the motion of GPS (Global Positioning Systems) satellites so as to continuously monitor and update their positions. Also, there is a need to create radiation nulls along certain spatial directions for an antenna transmitter/receiver to warrant secure and covert communications. Impedance control over boundary layers is required so that interrogation of the synthesized surface impedance becomes no more trivial. Other applications can be found in target searching/tracking radars, satellite communication systems, and TV program broadcasting antennas installed with a civilian jet carrier.

In a phased array system it is possible to include frequency-agile materials (varactors, ferroelectrics, and ferrites) to tune and adjust the phase and amplitude of each individual element so as to compose and tailor the overall radiation into a desirable pattern. However, beam forming in this manner is expensive; depending on the speed, frequency, and angle of steering, each phase-shifting element can cost as much as $1,000, and in a system containing 10,000 elements, the cost of the antenna array system can be formidable. Power dissipation is another consideration, since amplifiers are used following each of the phase shifting processes to compensate signal propagation loss, or insertion loss. To avoid overheating, water cooling is, therefore, often required in a large phased array system.

A radiation beam can also be steered via mechanical means, as commonly observed for a traffic radar installed at the airports. However, steering in this manner is slow, suffering from potential mechanical breakdowns. To incorporate free rotation, the antenna take up considerable space and the shape of the antenna is not conformal. As such, it is unlikely to apply a mechanically rotating radar in a body moving at high speed.

A reflect-array antenna operates in the same manner as an optical grating device: The reflected beam is constructed coherently from each of the array elements according to its reflection phase and electric path [Berry, D.G., et al, IEEE Transaction Antennas and Propagation, vol.11, pp.645-651, 1963].

Therefore, by adjusting the phase and/or electric path of the reflecting elements the overall beam construction can be controlled and manipulated, not only in its reflection direction, but also in its geometric shape, for example, beam width, side-lobe locations, and nulling directions.

The impedance of an active reflector surface can be tuned so that upon interrogation it can vary at arbitrary values. The surface impedance is subject to electronic tuning in two dimension, allowing both of its real part and imaginary part to change, simultaneously and independently. In other words it needs to tune over two real parameters to completely control the surface impedance, which may be taken as the permittivity and the permeability of the surface layer of the reflector, for example. As such, ferroelectric and ferrite materials are included with the reflector surface, and electric voltage and magnetic field are applied to change the permittivity and the permeability of the surface layer, thereby changing the surface impedance of the reflector electronically in two dimension.

For the research program specific active reflectors are proposed, capable of electronically configuring its local areas for desired electronic properties thereby providing beam-steering/beam-forming/beam-nulling functions and control over the surface impedance in two dimension. No amplifier is required and hence the problem of power dissipation is minimized. The reflector has a low profile containing no parts for mechanical rotation. The response time is fast and its fabrication is inexpensive.


## SUMMARY OF WORK

We have successfully accomplished the research goals set up in the proposal of the program relating to implementation of microwave active nulling. In order to actively manipulate a radiation beam so as to create microwave nulling a reflector surface is deployed upon which the reflection amplitude and phase of the incident wave can be controlled via electronic means. To do this both the local impedance and phase at various spots of the reflector surface are subject to electronic tuning by imposing a bias voltage and/or a bias current, for example. This allows the local permittivity and permeability of the reflector surface to vary, respectively. Frequency agile materials such as ferroelectric and ferrites are thus needed, and only if both of the ferroelectric and ferrite materials are utilized can the local permittivity and permeability of the reflector surface be simultaneously and independently adjusted.

In performing electronic-tuning functions resonant structures are utilized to enhance sensitivities in operation. Resonance can be extrinsic or intrinsic in nature, such as dimensional resonance or ferromagnetic resonance (FMR), respectively. Therefore, the bias voltage and the bias current are distinguished in two parts. Permanent biases are referred to those bias fields providing constant global background values to bring about the necessary resonant conditions, thereby facilitating the tuning operation. Superimposed with the background biases local variable fields are thereof imposed capable of modifying the background values in small scales at ease. This warrants high-speed operation. A magnetic background bias can be achieved by using a permanent magnet generating a sufficient magnetic field over a wide area with uniformity. Helmholtz coils are then used to induce local variable changes in the overall magnetic bias field. An electric background bias can be realized via the use of a constant voltage supply, and local fields are then added to the background field using variable

voltage sources to fine tune the overall electric bias field.

In order not to interfere with the RF properties of the reflector circuit DC bias electrodes are included with the resonance structure in a manner invisible to microwave propagation. That is, the bias electrode are made of thin conductor layers whose thickness compares negligibly small to the skin depth in the conductor. As such, high DC voltage up to 1000 V has been successfully expressed onto the reflector surface inducing sufficient change in permittivity. Furthermore, no soldering is required by the DC bias circuit and the bias electrodes are pressed against the resonator container walls in a straightforward manner. The employed bias electrode was cut from a commercial resistive sheet containing a gold layer of thickness 900 A deposited on top of a mylar layer.

Universal instrumentation has been fabricated allowing both the permittivity and the permeability measurements to be performed using the same equipment. Measurement instrumentation includes a coax-cable resonator whose boundary layer consists of frequency-agile materials, such as ferroelectric and ferrites. Electrodes and coils, which are required to generate the bias electric field and the bias magnetic field, respectively, are included with the measurement instrumentation, thereby causing the electronic properties of the boundary layer to change. Permanent magnet is also included so as to supply a magnetic bias background. The reason that a coax-cable resonator was chosen as the research candidate is that a coax cable supports TEM mode propagation of electromagnetic waves. This simulate the real situation, since a microwave reflector is normally used to receive the radiation waves in the far-field regime.

Two kinds of ferroelectric materials were used in measuring the permittivity changes induced in the boundary layer of the fabricated coax-cable resonator. They were both BST samples ($Ba_xSr_{1-x}TiO_3$: $x = 0.5$) obtained from Army Research Laboratory, Adelphi, MD, and from NZ Technology, Woburn, MA. While the Army sample is bulk BST of thickness 0.017", NZ sample is single crystal BST of thickness 0.4 $\mu$m grown on crystal $LaAlO_3$ substrate whose thickness is 0.02" and dielectric constant 10. Magnetic permeability measurements were performed with respect to garnet samples, G475 and G1010, which were purchased from Trans Tech, Adamstown, MD. The reflection data from the cavity resonator were analyzed rigorously. That is, instead of imposing the first order perturbation theory assuming the thickness of the included frequency agile material at the boundary layer is small, we have applied the transmission-line theory to explicitly calculate the effective thicknesses of the boundary layer. We note that the perturbation theory fails if a dielectric/magnetic sample is placed near an/a electric/magnetic wall, and explicit calculations must be applied to consider high-order effects. This is because, near an/a electric/magnetic wall electric/magnetic field vanishes, thereby invalidating the first-order expressions.

Traditionally, the measured reflection data from a resonator are analyzed with respect to a single resonance mode, assuming that mode does not couple to the other modes. In contrast we have analyzed the reflection data treating the whole spectrum of excited modes as a whole. It is necessary, because we found that the intrinsic resonance modes from the resonator couple to the other extrinsic modes forming standing modes inside the resonator. For example, at some frequencies standing modes are found in association with the boundary layer whose presence shifts considerably the resonance modes of the resonator. By plotting the measured resonance frequencies as a function of

the modal number of the resonator, the shift in resonance frequencies can thus be visualized. The intrinsic modes of the resonator can thus be analyzed using interpolation, removing effectively the coupling effects due to the other extrinsic standing modes.

The measured dielectric constant for the Army samples was 330, and for the NZ samples it was 10.8. The measured fractional changes in permittivity was +0.3 for the Army samples and -0.1 for the NZ samples upon the application of a DC bias voltage of 600V and 800V, respectively. For magnetic samples we found that permeability changed significantly when FMR conditions were approached. Our calculations compared nicely with measurements.

In the report a boundary layer were studied indirectly, whose electronic properties were inferred via analyzing the measured reflection data from a resonator containing the layer as the boundary wall. There is a need to directly measure the electronic properties of the boundary layer. For example, in the RF interrogation process the electronic properties of the boundary layer are directly accessed, not involving a structural resonator in mediation. Also, there is need to analyze the loss behavior of the boundary layer, as well as its effects in influencing the reflection data from a resonator. For these purposes TRL calibration techniques need to be employed along with the reflection measurements, excluding the unwanted effects of the coupling connectors from the scattering-parameter data, for example. Furthermore, the orchestral effects due to a ferroelectric layer and a ferrite layer applied concurrently in a boundary layer needs to be investigated, exploring the profound coupling of one material in interaction with the other, and vise versa. All of these important issues will be pursued in this continuation research program.

## IMPORTANT FINDINGS FROM THE RESEARCH AND DEVELOPMENT

Important findings of our performed research and developments are summarized in this section. Please refer to the following section for detailed data exhibition and outlining. Fig.1 shows the configuration of an active reflector. In Fig.1 microwave radiation is incident upon the reflector, which contains a ferrite layer (purple color) and a ferroelectric layer (orange color) as constituents. The permanent magnet provides a common magnetic bias so that the FMR conditions can be readily approached, thereby facilitating sensitive magnetic tuning. Dielectric Coating layer serves as a dimensional resonator to further assist the tuning sensitivity. Electric bias is applied via a thin electrode (yellow color) whose thickness comparing negligibly small
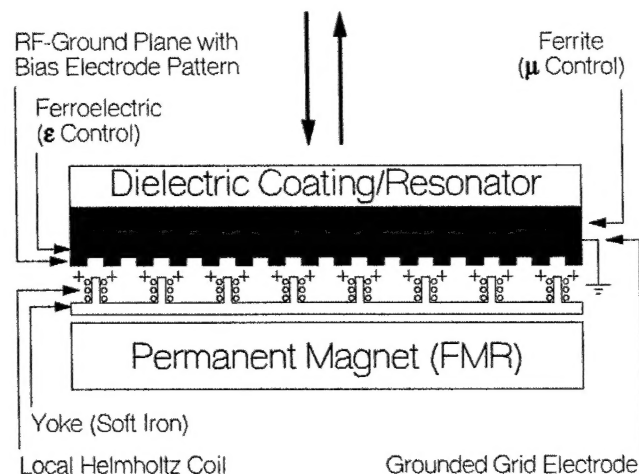


**Figure 1** Configuration of an active reflector.

to the skin depth in the conductor. As such, microwave radiation penetrates across this thin electrode with little attenuation, arriving at a patterned RF ground plane which also serves as the positive electrode for the DC bias. As such, the permittivity $\epsilon$ of the ferroelectric layer can be electronically tuned in local areas. Helmholtz coils, which wind around a common soft-iron yoke, are used to provide local tuning in the permeability $\mu$ of the ferrite layer. As a result, the local impedance of the reflector surface can be tuned in two dimensions, independently and simultaneously.

Fig.2 shows schematically the fabricated measurement apparatus of an active reflector under electric bias. In order to simulate the far-field radiations received by a microwave reflector deployed in true

**Electric Bias**



**Figure 2** Measurement apparatus of an active reflector under electric bias

situations measurements are carried out in a coax cable supporting TEM-mode wave propagation. The apparatus includes a grid electrode upon which positive voltages can be applied biasing onto the donut-shaped ferroelectric sample inducing permittivity changing. The terminology "grid electrode" is used in analogy to the grid electrode in an electron vacuum-tube: it allows bias voltages to be applied without necessarily blocking the flow of an electron beam. The grid electrode of Fig.2 consists of a gold layer of thickness 900A deposited on a mylar layer. Therefore, the grid electrode in Fig.2 is so thin that electromagnetic waves can penetrate through it without experiencing much attenuation. The ferroelectric sample is shown in red color in Fig.2, and the grid electrode is shown in yellow color. The RF ground plane, which is shown in light-green color in Fig.2, serves also as the negative-voltage electrode for the DC bias. A pin insulator, which is shown in purple color, is shown in Fig.2 enabling electric isolation for the applied DC bias voltage; otherwise the DC high voltage will conduct into the network analyzer during reflection measurements, thereby causing damage to the equipment. The pin insulation also forms a cavity resonator in the coax cable, which plays the role of the dielectric coating/resonator shown in Fig.1. Note that in Fig.2 the DC bias is applied by pressing the



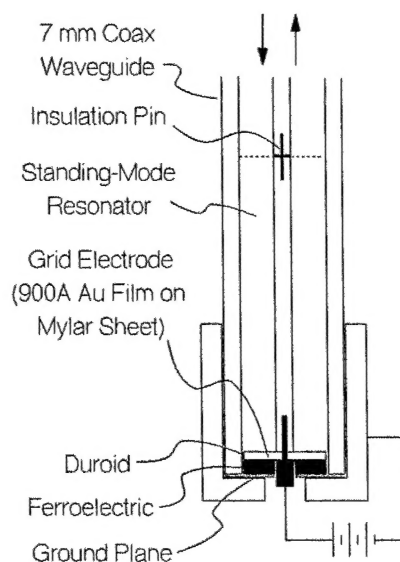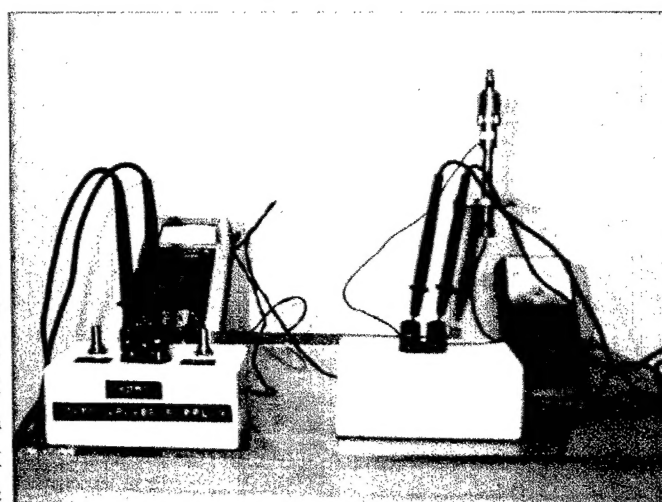**Figure 3** Fabricated measurement apparatus of an active reflector under electric bias. The home-made high-voltage supply is shown with annotation.

electrodes against coax cable conductors, central conductor and outer-wall conductor, none of which require soldering contacts, and hence it is convenient to apply. A photo picture of the fabricated measurement apparatus is shown in Fig.3. In Fig.3 the home-made high voltage supply is able to provide a bias voltage up to 1250 V, whose magnitude can be adjusted by turning two knobs in Fig.3 for coarse control (left) and for fine control (right), respectively.

Instead of using the first-order perturbation theory we have developed the rigorous analytical expression for the effective thickness of a sample layer placed inside a microwave cavity resonator. That is, when the sample layer is placed in the cavity resonator, the effective thickness of the layer changes, resulting in shift of the resonant frequencies of the resonator. Therefore, by



$\varepsilon, \mu$

(Electric Wall)

$E_{in} = Ae^{-i\beta_0 x}$

$E_r = Are^{-i\beta x}$

$\rightarrow | t | \leftarrow$

$$r = \frac{z-1}{z+1} = \frac{\cos\beta t - jz\sin\beta t}{\cos\beta t + jz\sin\beta t} = -\exp(-2j\beta_0 t_{eff})$$

$$z = (\mu/\varepsilon)^{1/2}; \; \beta_0 = \omega/c; \; \beta = \beta_0(\varepsilon\mu)^{1/2}$$

Perturbation Theory ($\beta t \ll 1$):

$t_{eff} = t\mu$, if material backed up by an electric wall

($t_{eff} = t\varepsilon$, if material backed up by a magnetic wall)

**Figure 4** Rigorous theory solving the effective thickness of a sample layer placed inside a cavity resoator.

measuring the shift in resonant frequencies of the resonator electronic properties of the sample layer, such as permittivity and permeability, can be ascertained. The rigorous formulation was developed using the transmission-line theory, since a coax-cable resonator supports TEM-mode wave propagation. In Fig.4 the sample layer is assumed to be placed near the boundary of the resonator where electric-wall boundary conditions are assumed. Similar expressions can be derived if the sample layer is placed elsewhere inside the cavity resonator. The reflection coefficient from the sample layer is set equal to the phase shift resulting from a traveling path whose length is twice the effective thickness of the sample layer. Under first-order perturbation, the mean-field theory results, and the effective thickness of the sample is weighted respectively by its permeability or permittivity value if electric-wall or magnetic-wall boundary conditions are assumed at the other side of the sample layer, please see Fig.4. We note that for the performed measurements the electric-wall boundary conditions were assumed and the perturbation theory failed to provide an answer for ferroelectric samples, since the first-order shift in the resonant frequencies of the resonator vanishes when a dielectric/ferroelectric sample is placed near a RF ground plane. Near a RF ground plane the tangential component of the electric field is zero as required by the boundary conditions. A rigorous theory is thus needed at least when dealing with dielectric/ferroelctric samples. We have used the rigorous formulation shown in Fig.4 to analyze the measured reflection data from the fabricated cavity resonator for both the ferroelectric and ferrite samples.

Fig.5 shows the measured spectra of resonant frequencies of the resonator when the Army sample, ARL, Adelphi, MD (one piece or two pieces), was inserted near the RF ground plane, please see Fig.2. Instead of measuring and analyzing a single isolated resonant mode, as adopted by a traditional analysis, we have chosen to analyze the whole set of spectrum of the resonant modes to resolve
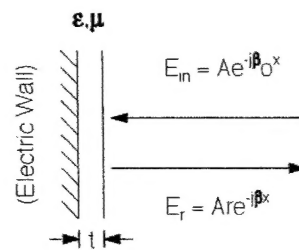
uncertainties, if any, associated with these modes. The reason for doing this is that a single resonant mode may couple to the other extrinsic modes existent in the cavity resonator. For example, as will be discussed shortly, standing modes were found to be excited within a ferrite sample of a sufficient thickness, and the measured resonant frequency of the resonator is thus not its intrinsic value. As such, erroneous answer can result if care is not taken. However, if the whole set of the spectrum of the resonant modes are analyzed instead this coupling effect due to external modes can be removed by interpolation, thereby furnishing a better accuracy.

By interpolating the measured resonant frequencies the effective thickness of the sample layer inserted inside the resonator can thus be determined, which, in turn,



**Figure 5** Resonant frequencies of the cavity resonator containing one/two piece(s) of Army BST sample.

gives rise to the permittivity and/or the permeability of the sample layer. Fig.6 shows two straight lines interpolated from the measured resonant frequencies of the resonator inside which one piece and two pieces of the Army sample was inserted, respectively, which is bulk BST ($Ba_xSr_{1-x}TiO_3$: x = 0.5)

of a thickness 0.017". From both of the slopes of the two interpolated straight lines shown in Fig.5 the calculated permittivity of the Army sample was 330, which compared closely to its quoted value of 285. When a bias voltage of 600V was applied across the two bias electrodes, the grid electrode and the ground plane shown in Fig.2, the permittivity of the BST sample changed, and the fractional change in permittivity was determined to be -0.3; please see the following section for detailed data exhibition and outlining. Analogously, the resonant frequencies associated with one piece and two pieces of the NZ sample are shown in Fig.6. The NZ sample consists of a single crystal BST ($Ba_xSr_{1-x}TiO_3$: x = 0.5) film of thickness 0.4 $\mu$m grown on top of a $LaAlO_3$ substrate whose thickness was 0.02" and dielectric constant was 10. From
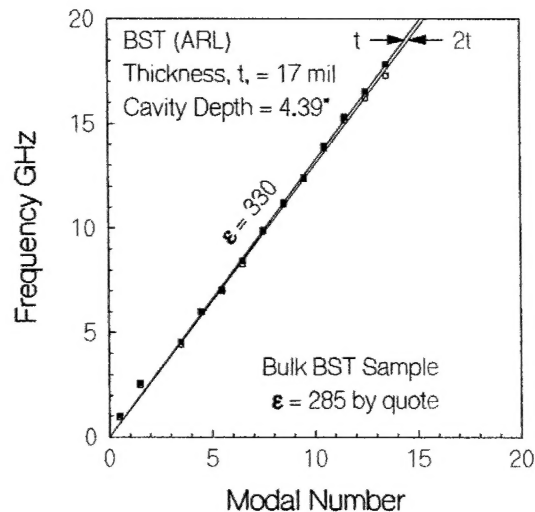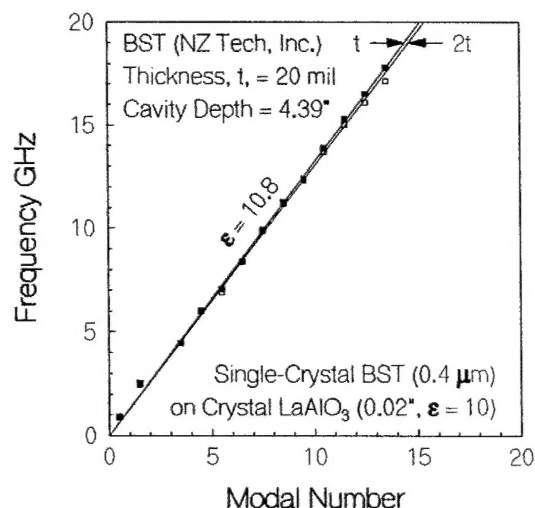


**Figure 6** Resonant frequencies of the cavity resonator containing one/two piece(s) of NZ BST sample.

the two interpolated straight lines in Fig.6 the permittivity of the NZ sample was determined to be 10.8, which compared nicely with its quoted value of 10.6. When a bias voltage of 800V was applied, the shifts in resonant frequencies determined the fractional change in permittivity of the NZ sample to be 0.1; please see the following section for detailed data exhibition and outlining. From Figs.5 and 6, we see that although the shift in resonant frequencies are small upon the application of a bias voltage, nevertheless, the developed formulation utilizing the transmission-line theory is effective in analyzing the measured reflection data from the fabricated coax-cable cavity resonator loaded with the Army and the NZ BST samples.
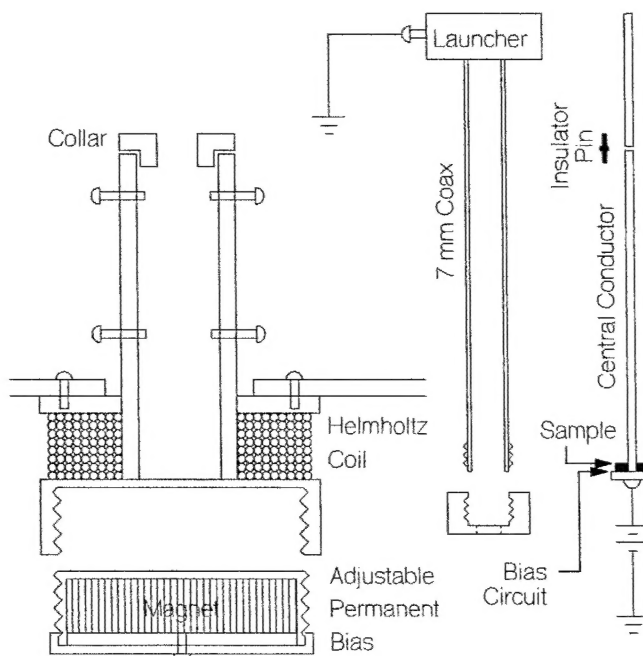


**Figure 7** Schematic of the fabricated measurement apparatus under magnetic bias.

Fig.7 depicts the fabricated measurement apparatus of an active reflector under magnetic bias. The apparatus includes a permanent magnet which was able to provide a constant background magnetic field up to 3365 Oe in the ferrite sample region. Helmholtz coil was also included with the measurement apparatus which was capable of generating a variable bias magnetic field up to ±230Oe in the magnetic sample region, i.e., the maximum bias current in the Helmholtz coil was 4A. The apparatus shown in Fig.7 can also be used to supply an electric bias, although only magnetic biases were exercised for the performed measurements. An insulation pin was inserted with the central conductor of the coax cable so as to electrically insulate the applied electric bias voltage. A cavity resonator was formed with the coax cable transmission line, whose role is in analogy to the dielectric coating/resonator shown in Fig.2. A photo picture of the fabricated measurement apparatus under magnetic bias is shown in Fig.8.

Fig.9 plots the measured resonant frequencies as a function of the modal number of the cavity resonator, and the resonator was loaded with a ferrite sample G475 under zero magnetic bias. The ferrite sample G475 was purchased from Trans Tech with the following parameters: $4\pi M_s = 475$ G, $\epsilon = 14.1$, $\Delta H = 200$ Oe. The ferrite sample was cut into a ring geometry of ID = 3 mm, OD = 7 mm, and thickness = 0.15". In Fig.9 it is
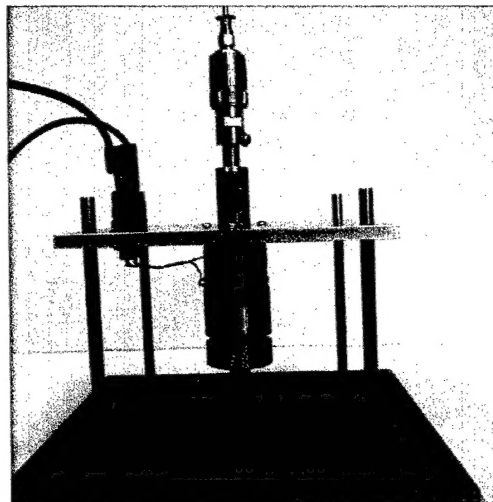


**Figure 8** Photo picture of the fabricated measurement apparatus under magnetic bias.
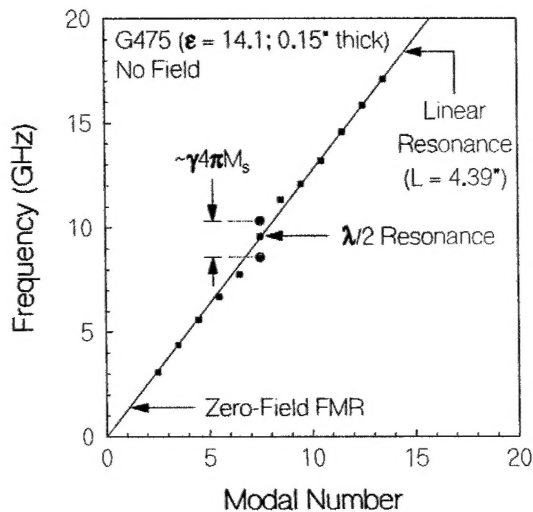
**Figure 9** Measured resonant frequencies plotted as a function of the modal number.
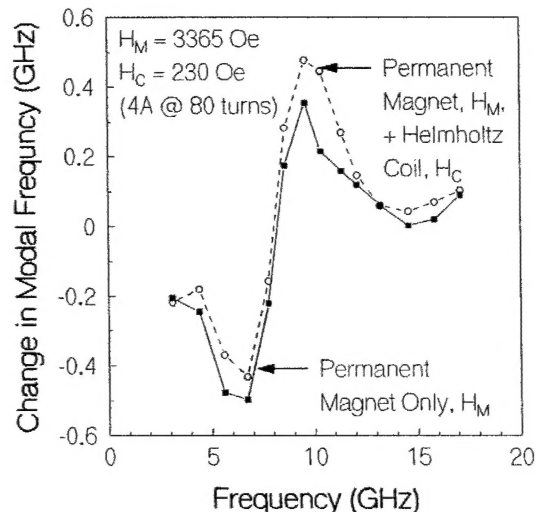
**Figure 10** Measured frequency changes when the ferrite sample is applied under magnetic bias.

seen that two extra modes appear near the modal number 7.5. These two extra modes were determined to be associated with the standing modes excited within the ferrite sample itself, namely, the $\lambda/2$ resonance. However, in contrast to a dielectric sa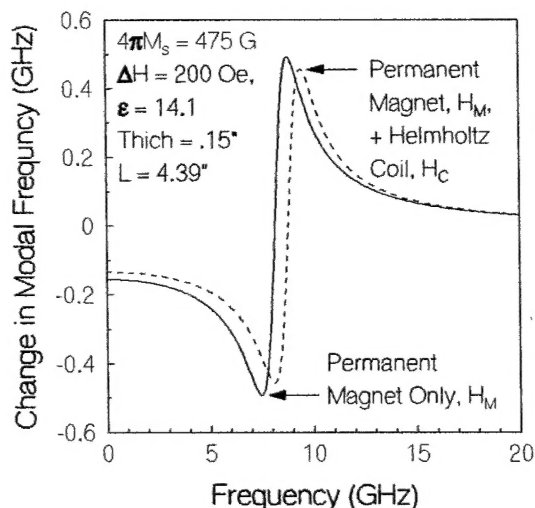mple, the degeneracy between the two standing modes with opposite senses in circular polarization was removed by the internal field of the ferrite sample, and the splitting between these two circularly polarized modes is roughly $\gamma 4\pi M_s$, where $\gamma$ denotes the gyromagnetic ratio. In Fig.9 it is seen that the $\lambda/2$ standing modes excited within the ferrite sample couple strongly to the resonant modes of the coax-cable cavity resonator, causing the latter to shift significantly for modal numbers near 7.5. However, as mentioned previously, by interpolating the measured resonant frequencies of the coax-cable resonator, this coupling effect can be effectively removed, and the effective thickness of the inserted ferrite sample can thus be determined using the developed transmission-line theory, please see Fig.4.

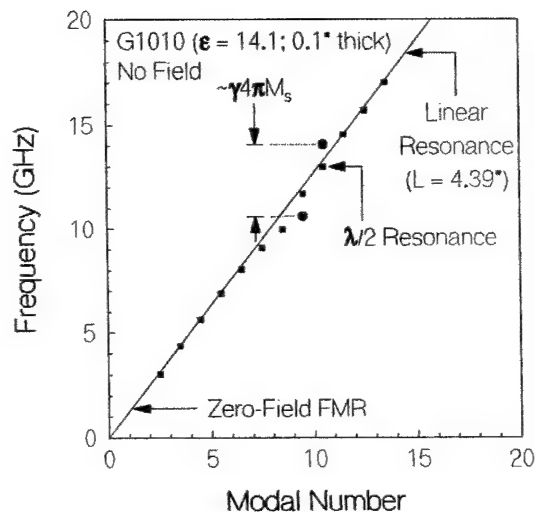Fig.10 plots the frequency changes in the resonant modes of the cavity resonator subject to magnetic



**Figure 11** Calculated frequency changes when the ferrite sample is applied under magnetic bias.

**Figure 12** Measured resonant frequencies plotted as a function of the modal number.
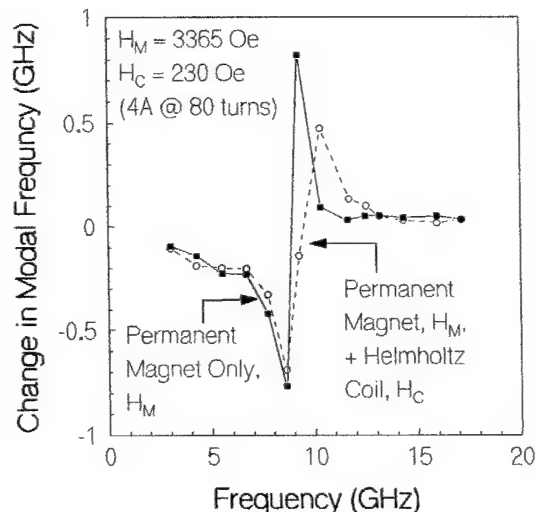
**Figure 13** Measured frequency changes when the ferrite sample is applied under magnetic bias.

biases. In Fig.10 the solid line is associated with the bias under the permanent magnet only and the dashed line under the permanent magnet plus the Helmholtz coil. Compared to electric bias applied to a ferroelectric sample, magnetic bias applied to a ferrite sample was more sensitive, giving rise to more pronounced changes in the resonant frequencies of the cavity resonator. This is because both of the samples were placed near the RF ground plane of the resonator producing a maximum tangential magnetic field but a negligible tangential electric field in the sample region. Fig.11 shows the calculated frequency changes when the ferrite sample G475 was placed inside the cavity resonator subject to magnetic bias: the solid line corresponds to bias under the permanent magnet only and the dashed line under the permanent magnet plus the Helmholtz coil. We note that in deriving these curves shown in Fig.11 no adjustable parameters were used in the calculations, and the permeability of the ferrite sample was assumed to be



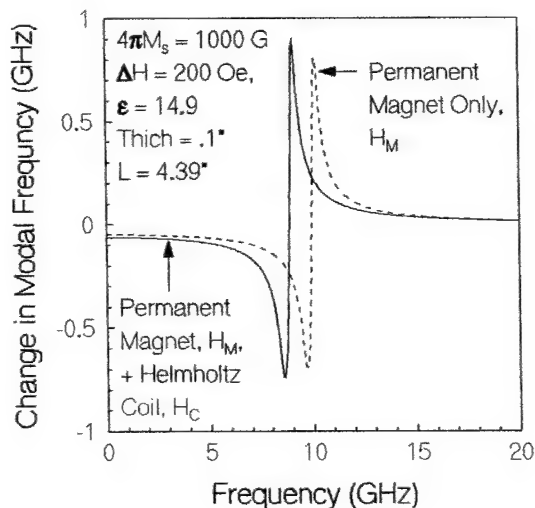$$\mu_{eff} = \frac{\mu_+ + \mu_-}{2} = 1 + \frac{4\pi M_s H_{in}}{(4\pi M_s)^2 - (f/\gamma)^2}$$

**Figure 14** Calculated frequency changes when the ferrite sample is applied under magnetic bias.

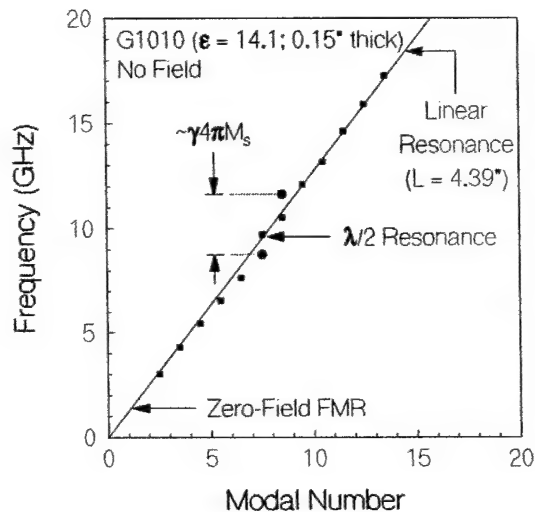Here $\mu_+$ and $\mu_-$ are permeability of Faraday modes

**Figure 15** Measured resonant frequencies plotted as a function of the modal number.
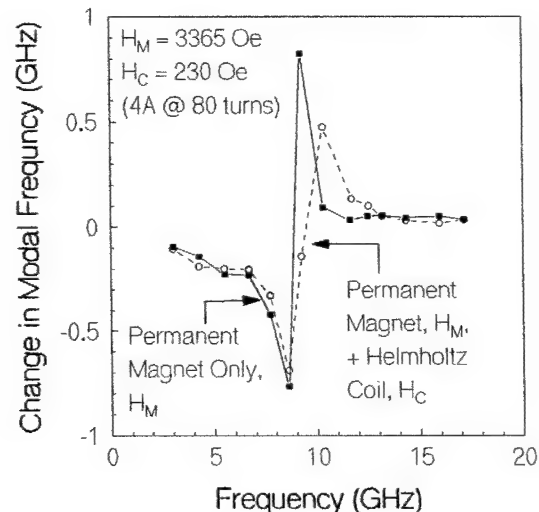
**Figure 16** Measured frequency changes when the ferrite sample is applied under magnetic bias.

characteristic of wave propagation along the applied field direction with left-hand and right-hand circular polarizations in ferrites, respectively, and $H_{in}$ is the internal field within the ferrite sample. Assuming the demagnetizing factor of the ferrite sample is close to 1, $H_{in}$ relates to the applied field $H_a$ by the following equation:

$$H_{in} \approx H_a - 4\pi M_s.$$

Comparing Fig.11 with Fig.10 we note that the agreement between theory and experiments is remarkable.
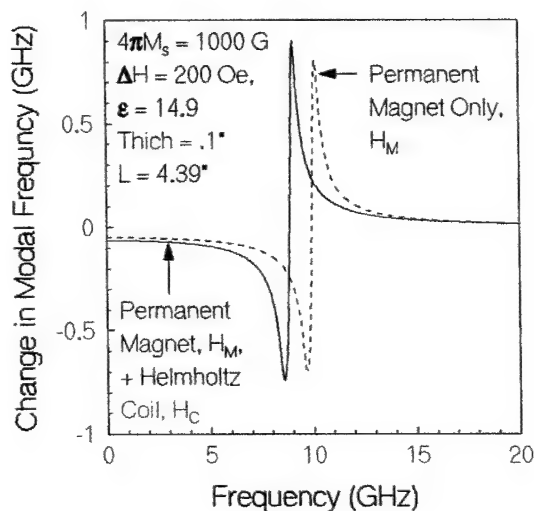


**Figure 17** Calculated frequency changes when the ferrite sample is applied under magnetic bias.

Fig.12 plots the measured resonant frequencies of the cavity resonator as a function of the modal number in the absence of a bias magnetic field. For the measurements associated with Fig.12 the cavity resonator was loaded with a ferrite sample G1010 purchased from Trans Tech. The ferrite sample was of a ring geometry characterized by the following parameters: $4\pi M_s = 1000$ G, $\epsilon =$ 14.8, $\Delta H = 200$ Oe, ID = 3 mm, OD = 7 mm, and thickness = 0.1". In Fig.12 two additional standing modes appeared near modal number 9.5 and 10.5, corresponding to the $\lambda/2$ resonance in the ferrite sample itself. However, when comparing to Fig.9

showing the same standing modes in a ferrite sample with a smaller $4\pi M_s$ and a larger thickness, the standing modes in Fig.12 shift to higher frequencies with larger mode splitting in frequencies, as expected. Fig.13 shows the frequency changes when the ferrite sample G1010 was applied under magnetic bias, and the solid curve correspond to the bias under the permanent magnet only and the dashed curve under the permanent magnet plus the Helmholtz coil. The corresponding curves from calculations are shown in Fig.14. Fig.15 shows measurements from the same ferrite sample material of thickness 0.15" under no magnetic bias. The two standing modes excited within the ferrite sample, say, the $\lambda/2$ resonances, occurred at lower frequencies, but showing approximately the same mode splitting in frequencies, please see Fig.12. This is because $4\pi M_s$ is the same but the thickness is now larger. When bias fields were applied, the changes in resonant frequencies are plotted in Fig.16 for bias under the permanent magnet only, the solid curve, and bias under the permanent magnet plus the Helmholtz coil, the dashed curve. The corresponding curves from calculations are shown in Fig.17. The magnetic linewidth used in the calculations of Fig.17 was $\Delta H = 1000$ Oe, which is larger than the quoted value of 200 Oe. This discrepance is due to the fact that the internal field is non-uniform within the ferrite sample, and the large $4\pi M_s$ and thickness of the sample result in an effective linewidth in the order of $4\pi M_s$. Calculations shown in Figs.11, 14 and 17 compared nicely with experiments, shown in Figs.12, 15, and 18, respectively.

## DETAILED DATA EXHIBITION AND OUTLINING

Purpose:

Phase/Impedance Control Over A
Boundary Layer Upon EM-Wave
Incidence/Interrogation

Key Element — Frequency Agile Materials

Ferrite: Magnetic Mean
Ferroelectric: Electric Mean

Local Resonator: Tuning-Sensitivity Enhance

# LOCAL PHASE/IMPEDANCE CONTROL OVER A BOUNDARY LAYER UPON TEM-WAVE REFLECTION

RF Ground Plane with Bias Electrode Pattern

Ferrite ($\mu$ Control)

Ferroelectric ($\varepsilon$ Control)

Dielectric Coating/Resonator

Permanent Magnet (FMR)

Yoke (Soft Iron)

Local Helmholtz Coil
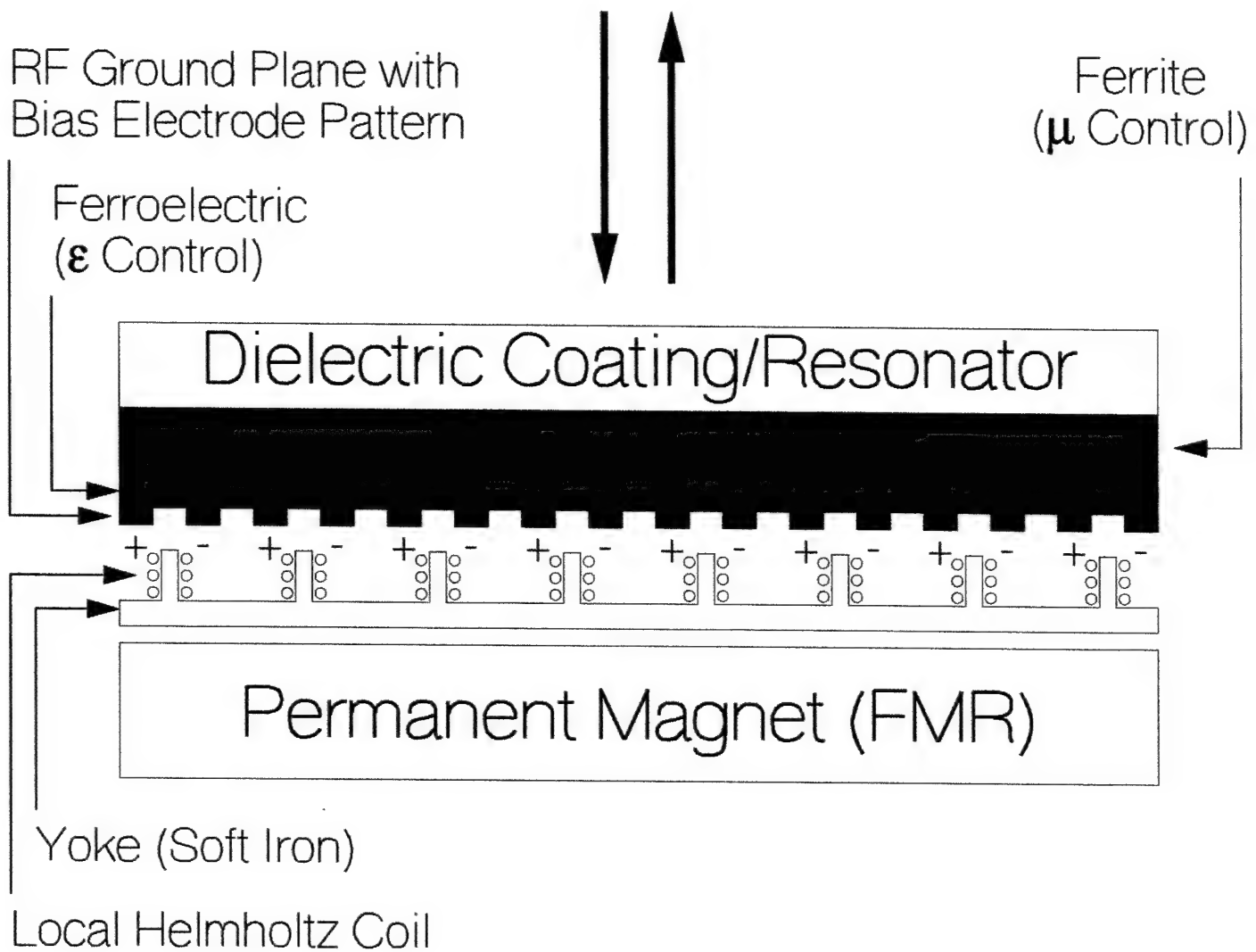
- Resonant Mechanism (Standing Mode / FMR)

- Wavelength is varying $\propto 1/\sqrt{\mu(H)\epsilon(E)}$

- Impedance is varying $\propto \sqrt{\mu(H)/\epsilon(E)}$

# LOCAL PHASE/IMPEDANCE CONTROL OVER A BOUNDARY LAYER UPON TEM-WAVE REFLECTION

RF-Ground Plane with
Bias Electrode Pattern

Ferrite
($\mu$ Control)

Ferroelectric
($\varepsilon$ Control)

Dielectric Coating/Resonator

Permanent Magnet (FMR)

Yoke (Soft Iron)

Local Helmholtz Coil

Grounded Grid Electrode
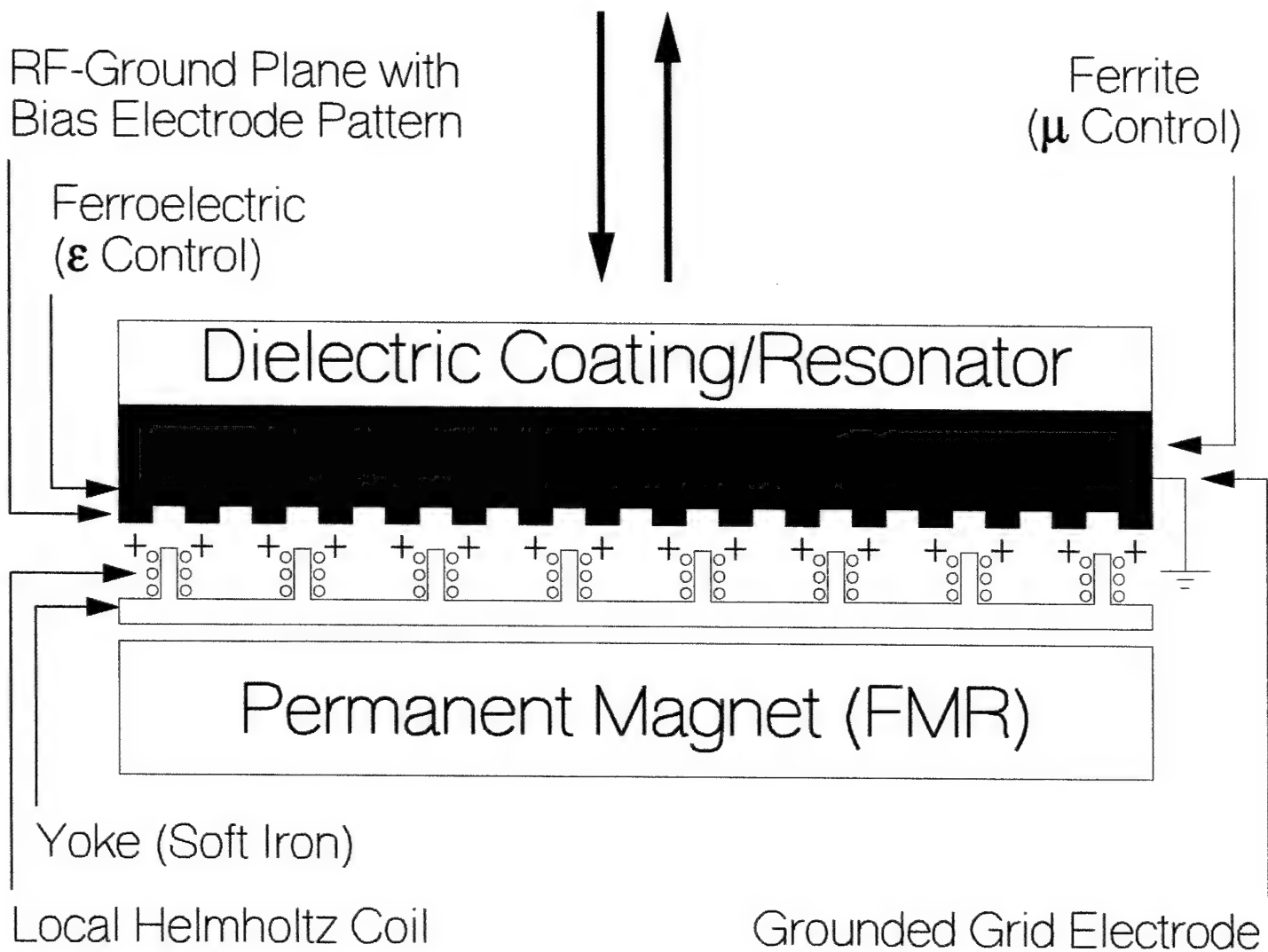
- Resonant Mechanism (Standing Mode / FMR)

- Wavelength is varying $\propto 1/\sqrt{\mu(H)\epsilon(E)}$

- Impedance is varying $\propto \sqrt{\mu(H)/\epsilon(E)}$

# Electric Bias

Fringing-Field Bias          Grid-Field Bias

7 mm Coax
Waveguide

Insulation Pin

Standing-Mode
Resonator

Grid Electrode
(900A Au)

Ferroelectric

Bias Circuit

Duroid

Ferroelectric

Ground Plane
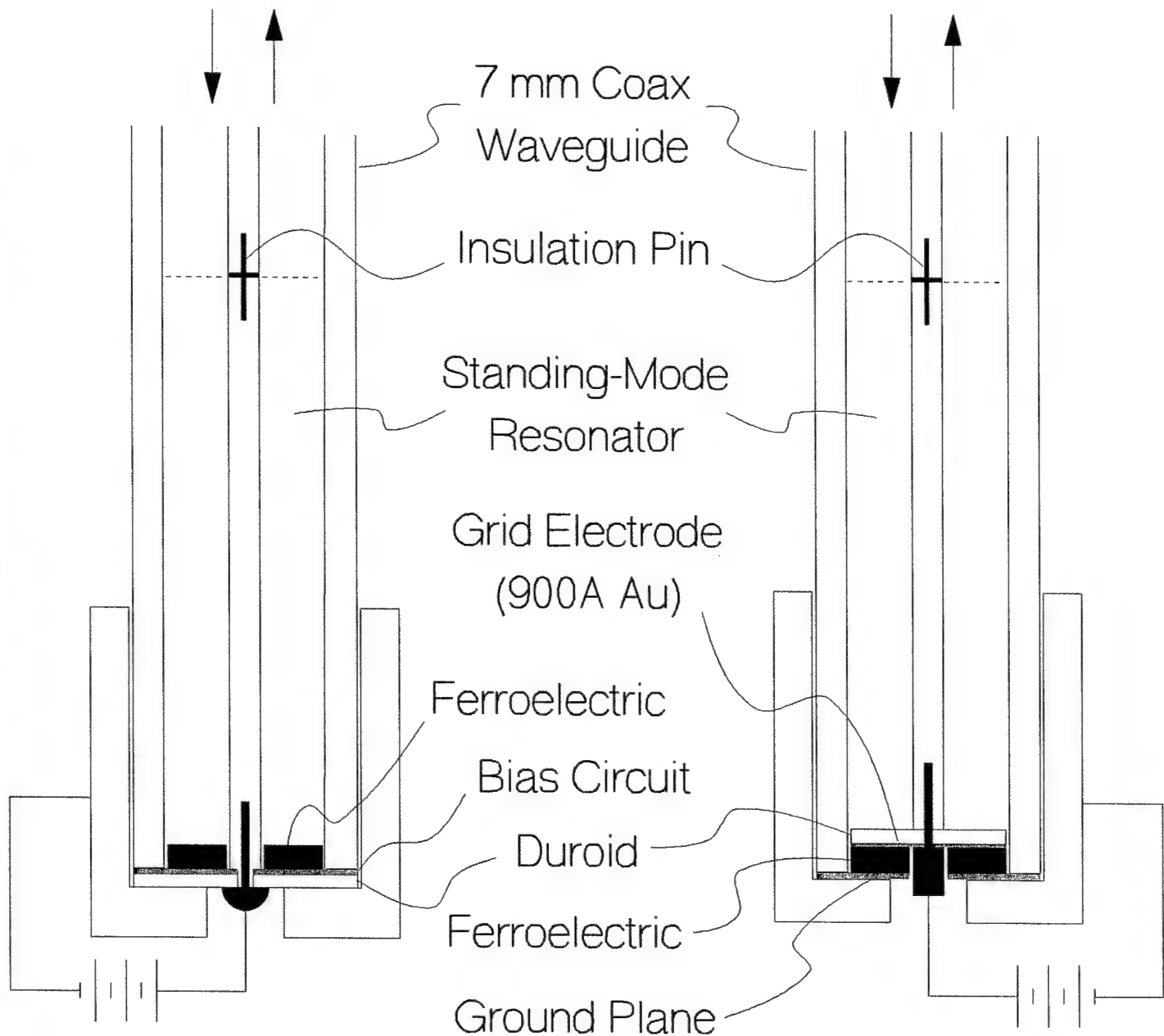
- BST Samples from ARO and NZ Tech.
- Fringing Field Creates Random Polarization
- At 20 GHz $\delta_{skin}$ = 7000 Å in gold

# Electric Fringe-Field Bias Circuit

- Interdigitated Electrodes
- Electrodes Run Parallel to RF e-Field
- Outer Electrode Connects to Coax Wall
- Inner Electrode Connects to Center Cond.
- Ring-Shaped Sample in Between
- Screw-Tight (No Soldering Required)
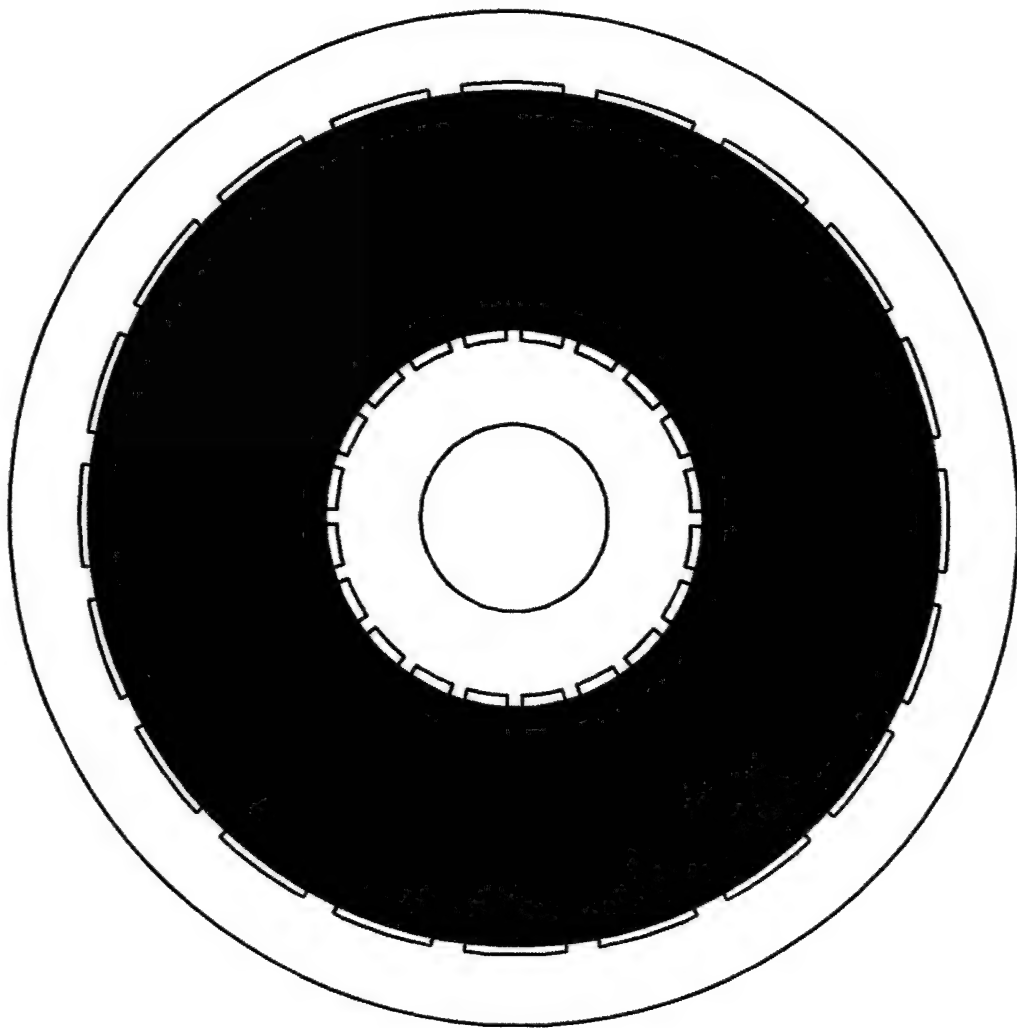
**Ground Plane with Fine Gratings**
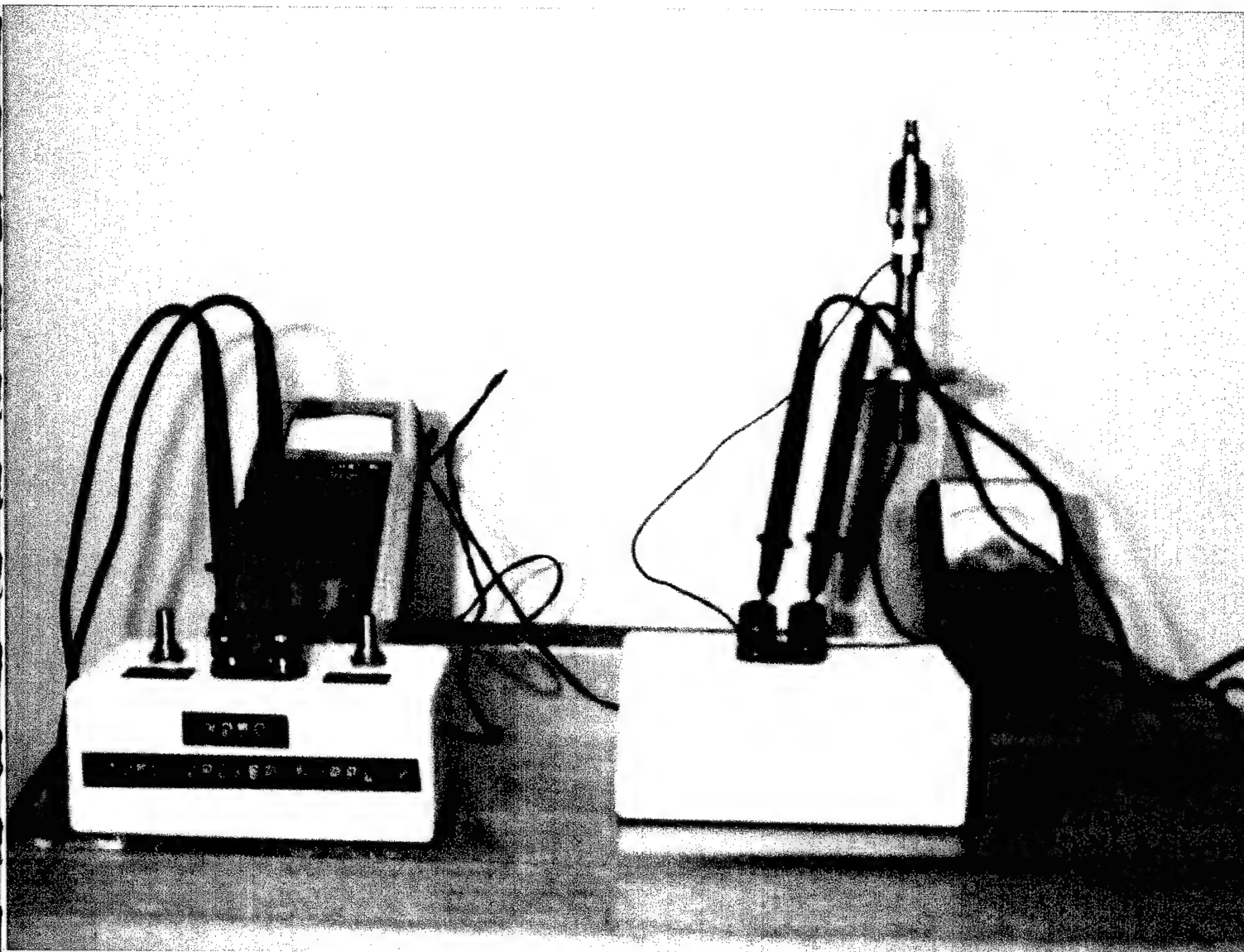
- Home-Made High-Voltage Circuit (1250 V)
  (Coarse Control and Fine-Scale Adjustment)
- Universal for providing Fringing-Field
  and Grid-Field Bias
- Convenient in Use (No Soldering Required)
- TEM-Mode Resonance with Electronically
  Controlled Boundary-Layer Impedance
  (Ring-Shaped Ferroelectric Sample)
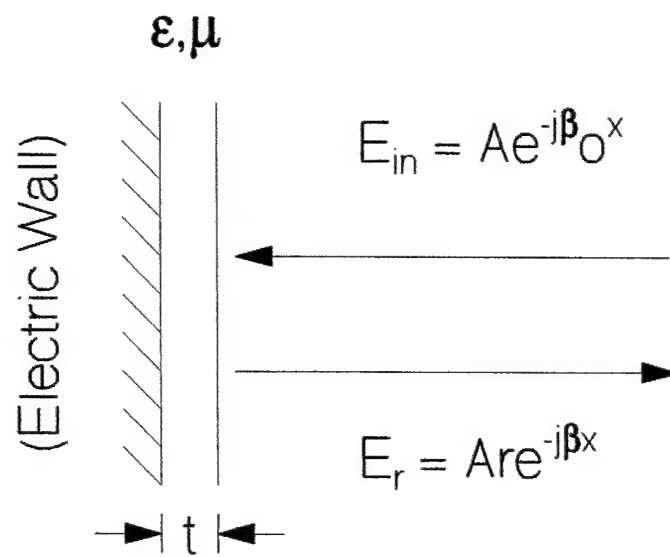
$$\varepsilon, \mu$$



$$r = \frac{z - 1}{z + 1} = \frac{\cos\beta t - jz\sin\beta t}{\cos\beta t + jz\sin\beta t} = -\exp(-2j\beta_0 t_{eff})$$

$$z = (\mu/\varepsilon)^{1/2}; \quad \beta_0 = \omega/c; \quad \beta = \beta_0(\varepsilon\mu)^{1/2}$$

Perturbation Theory ($\beta t \ll 1$):

$t_{eff} = t\mu$, if material backed up by an electric wall

($t_{eff} = t\varepsilon$, if material backed up by a magnetic wall)

- **Rigorous Analysis**
- **Transmission-Line Analysis**
- **High-Order Effects (Mean-Field Theory not applicable for Dielectric Measurements)**

S11
REF 0.0 dB
10.0 dB/

log MAG

S11
REF 0.0 °
50.0 °/

∠
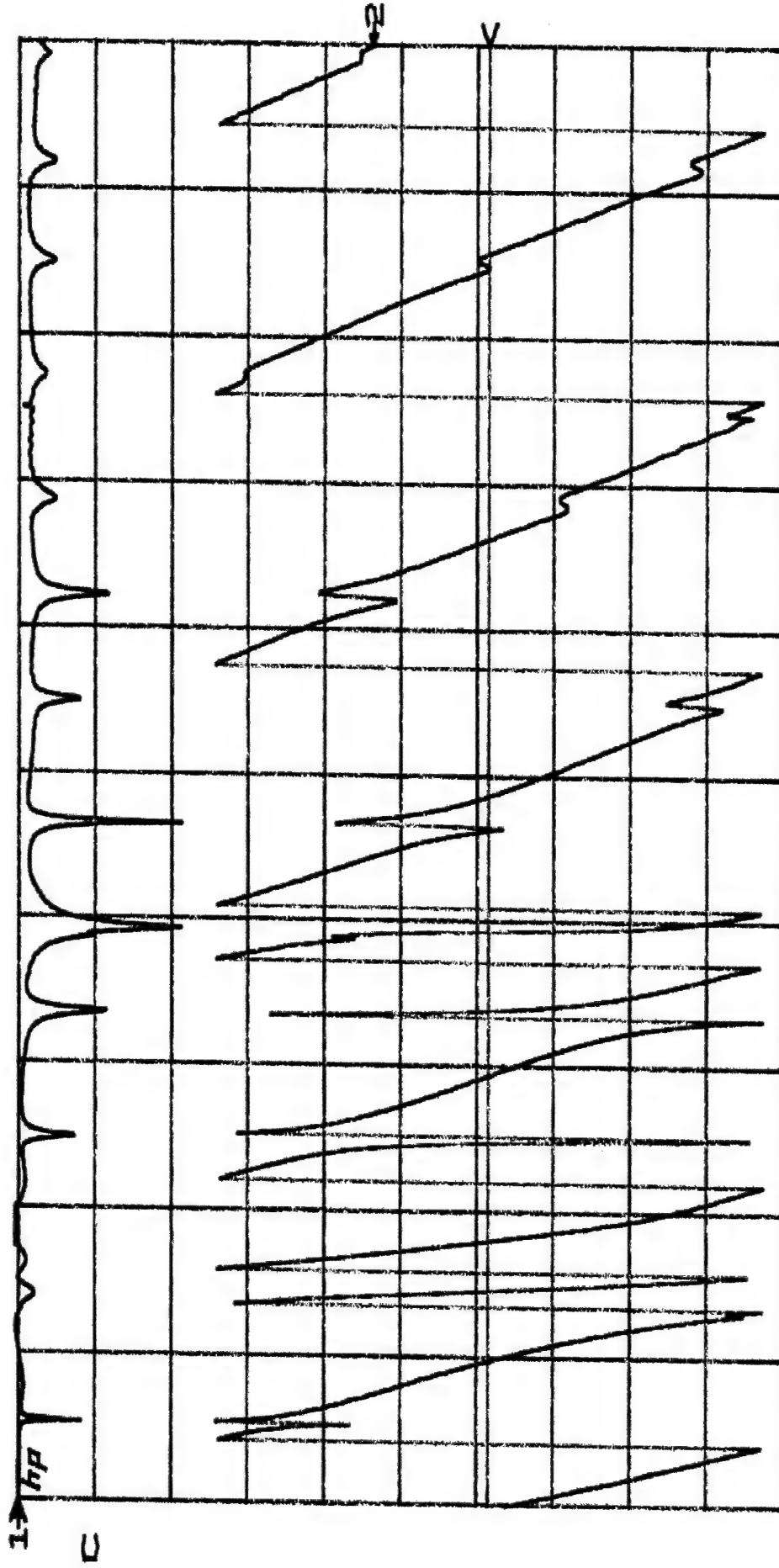
START    0.045000000  GHz
STOP    18.000000000  GHz

Measured Phase and Amplitude on One Piece of AF Sample at $V_{bias} = 0$ V.
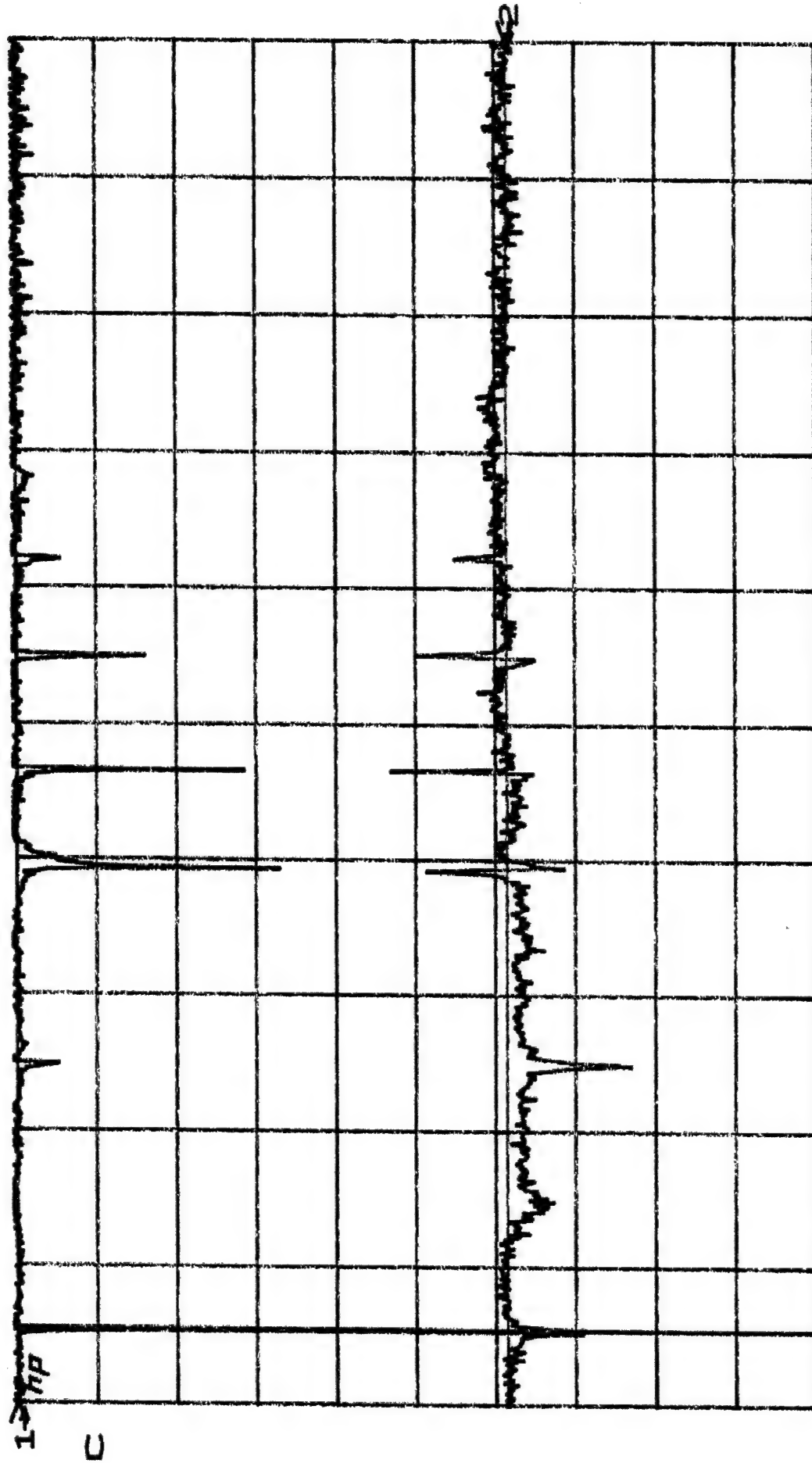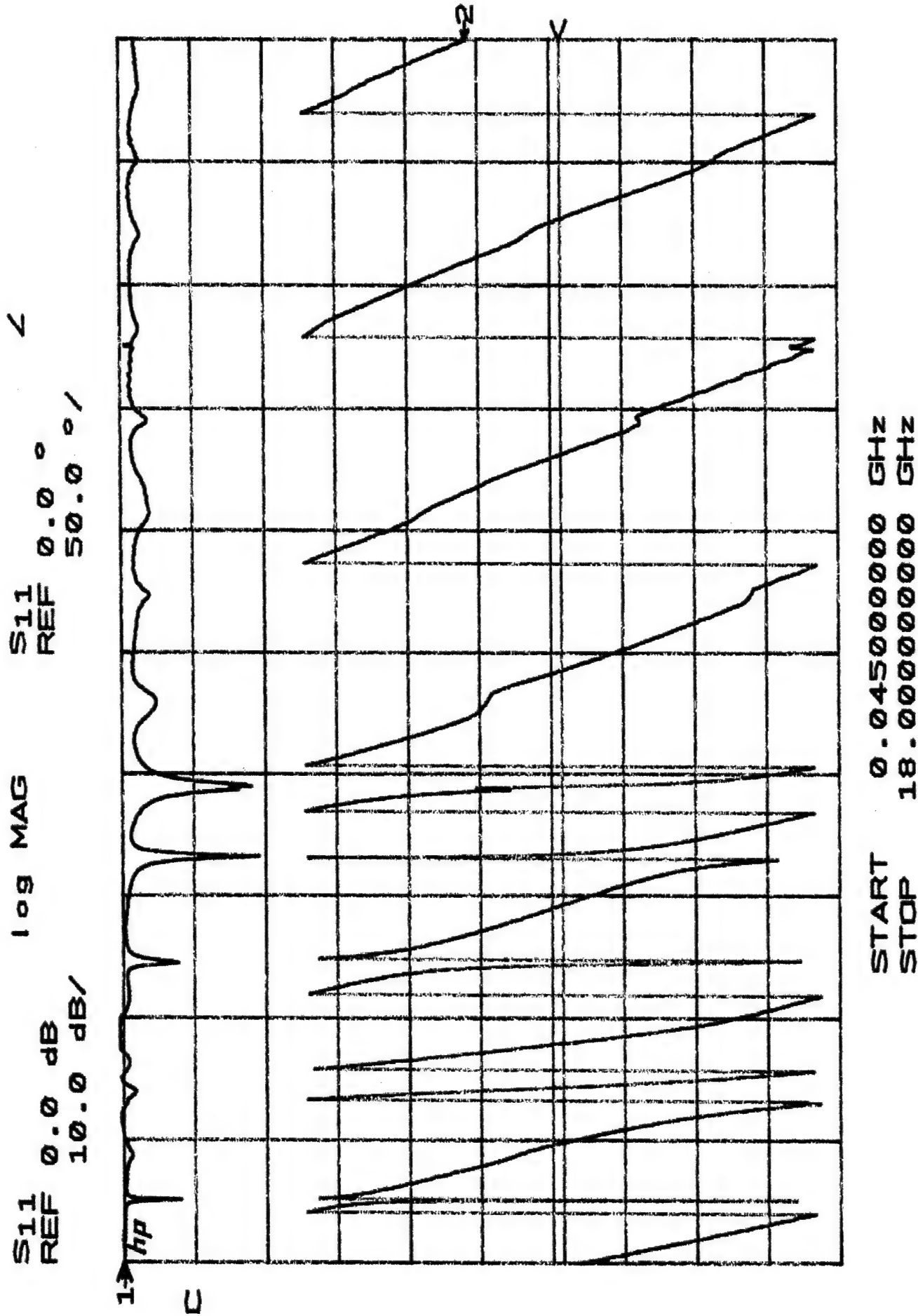
Normalized Phase and Amplitude on One Piece of AF Sample at $V_{bias} = 600$ V.

Measured Phase and Amplitude on Two Pieces of AF Sample at $V_{bias} = 0$ V.
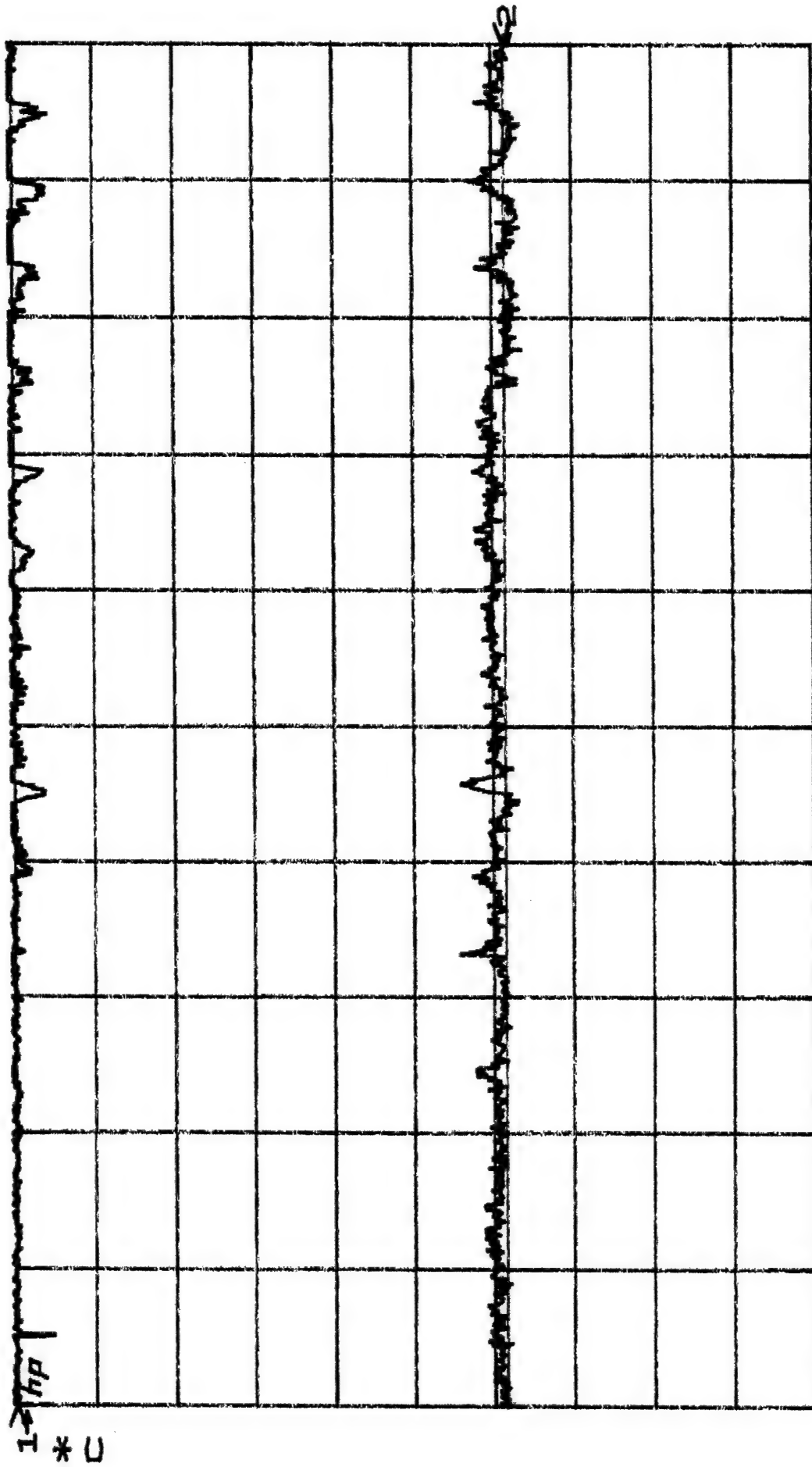
Normalized Phase and Amplitude on Two Pieces of AF Sample at $V_{bias} = 600$ V.
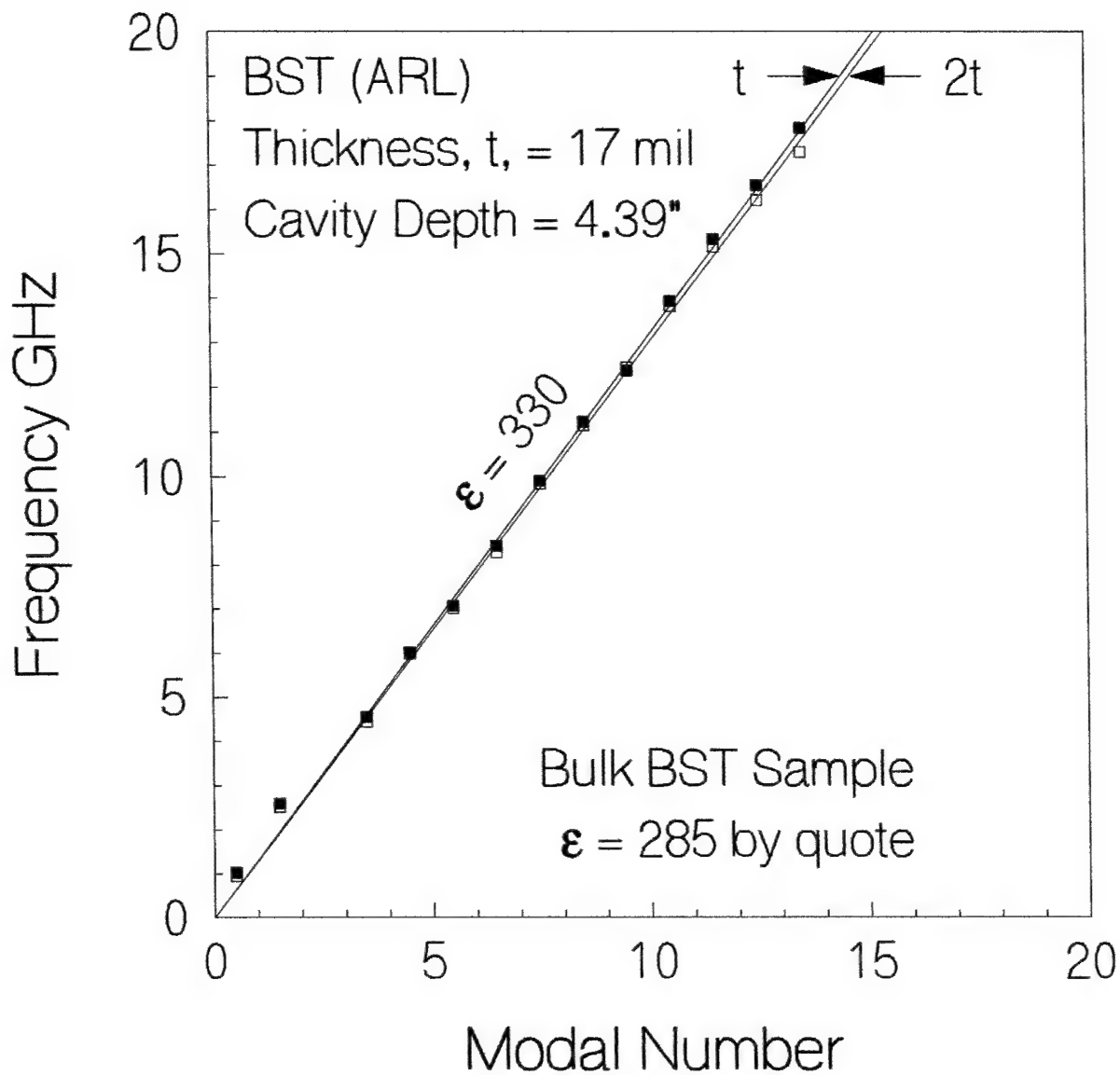
- Modal Spectra Analysis on One/Two Piece(s) of ARL Sample (Adelphi, MD) at $V_{bias} = 0$ V
- Full Transmission-Line Analysis Employed
- Perturbation Theory Not Applicable
- Less Electronic Tuning Than Expected
- $\Delta\epsilon/\epsilon \sim -0.3$ at $V_{bias} = 600$ V
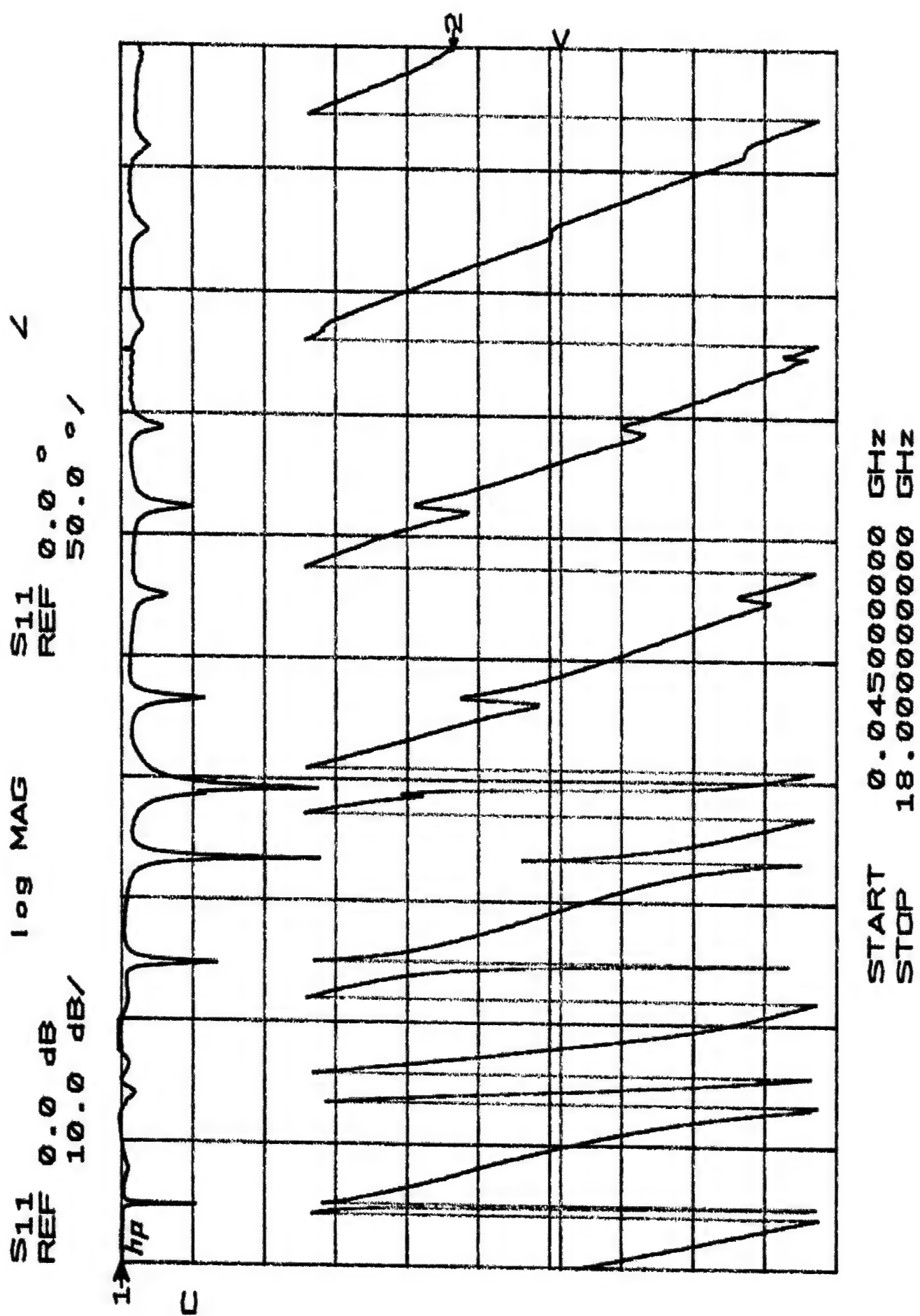
Measured Phase and Amplitude on One Piece of NZ Sample at $V_{bias}$ = 0 V.
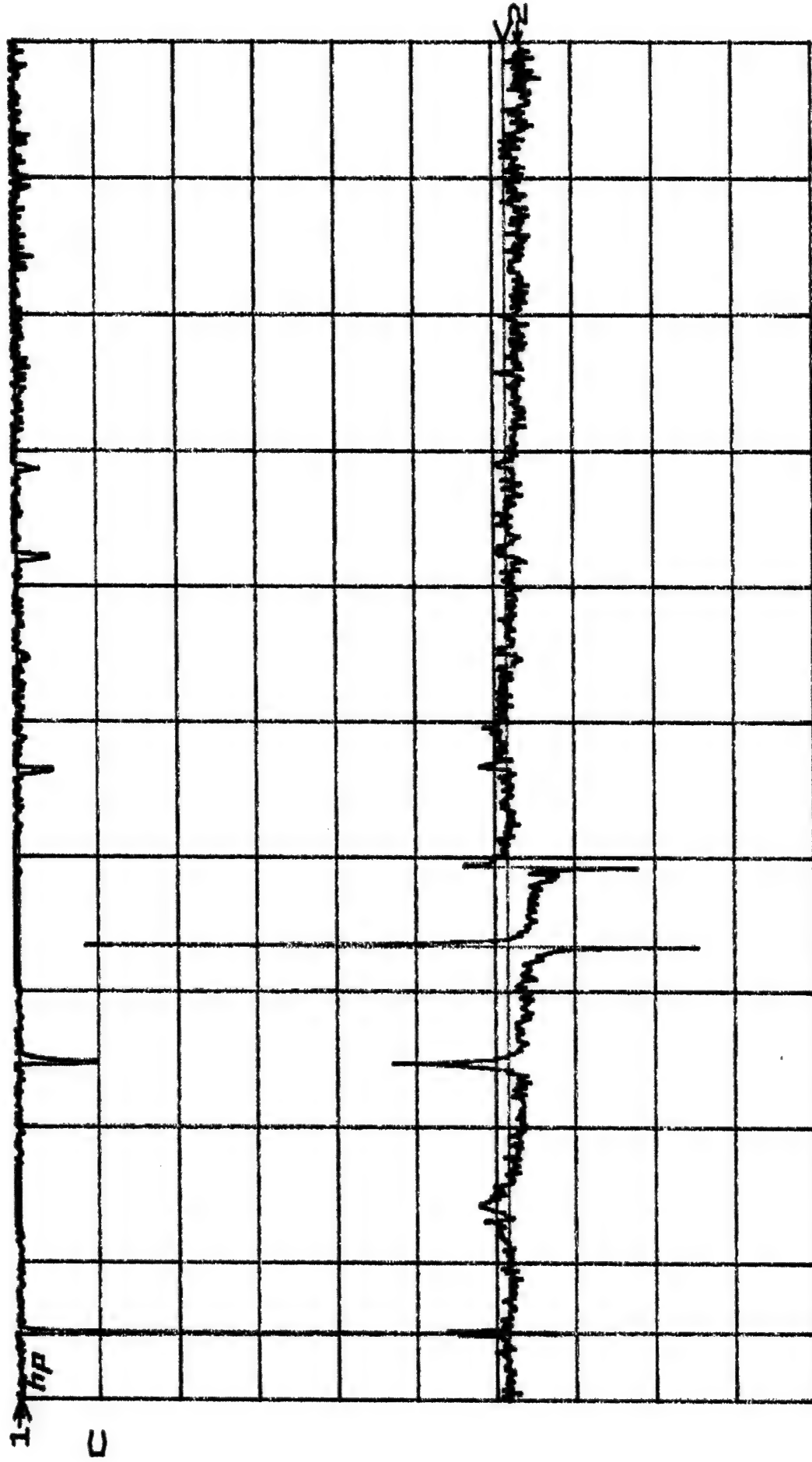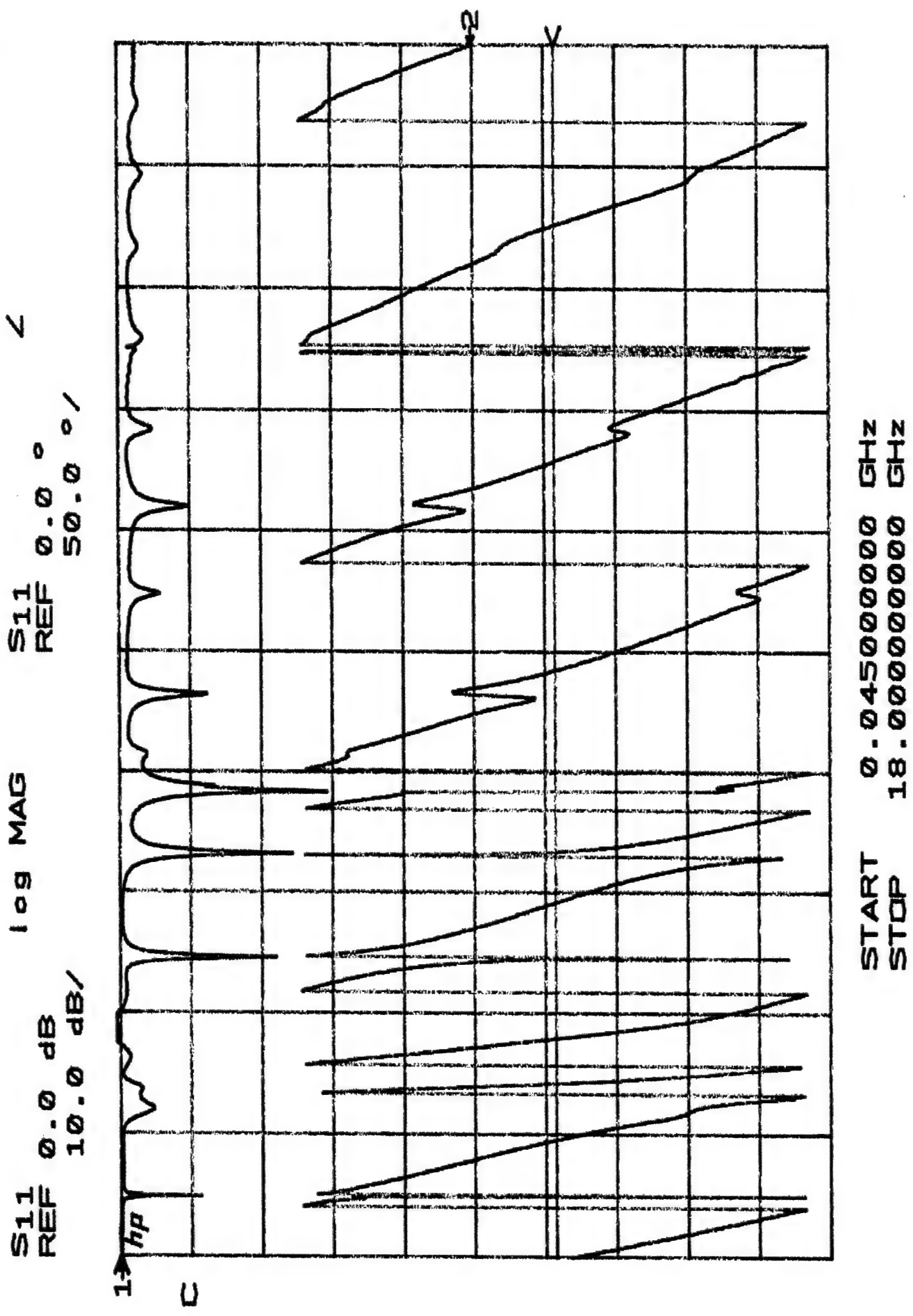
Normalized Phase and Amplitude on One Piece of NZ Sample at $V_{bias}$ = 800 V.

Measured Phase and Amplitude on Two Pieces of NZ Sample at $V_{bias} = 0$ V.
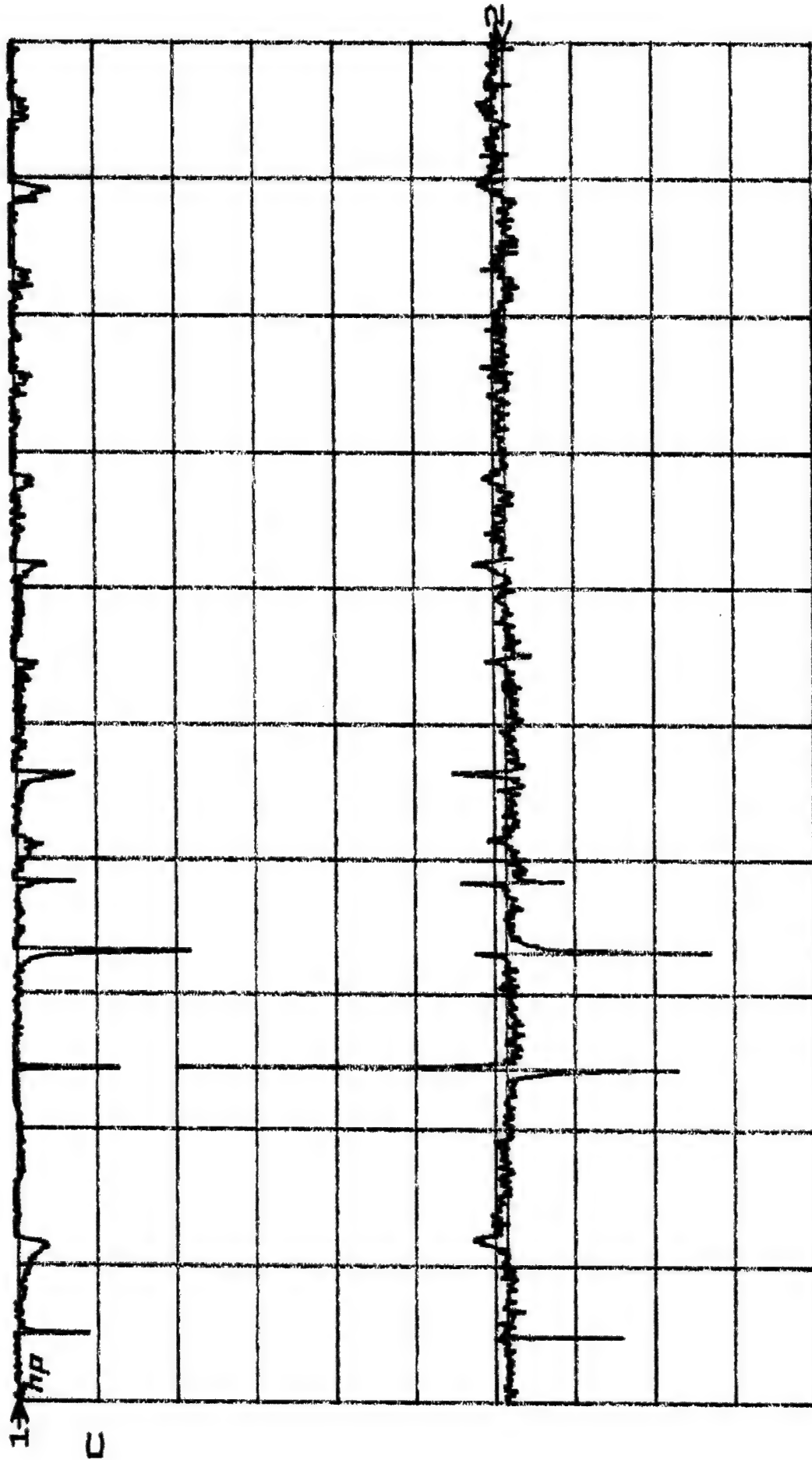
Normalized Phase and Amplitude on Two Pieces of NZ Sample at $V_{bias} = 800$ V.
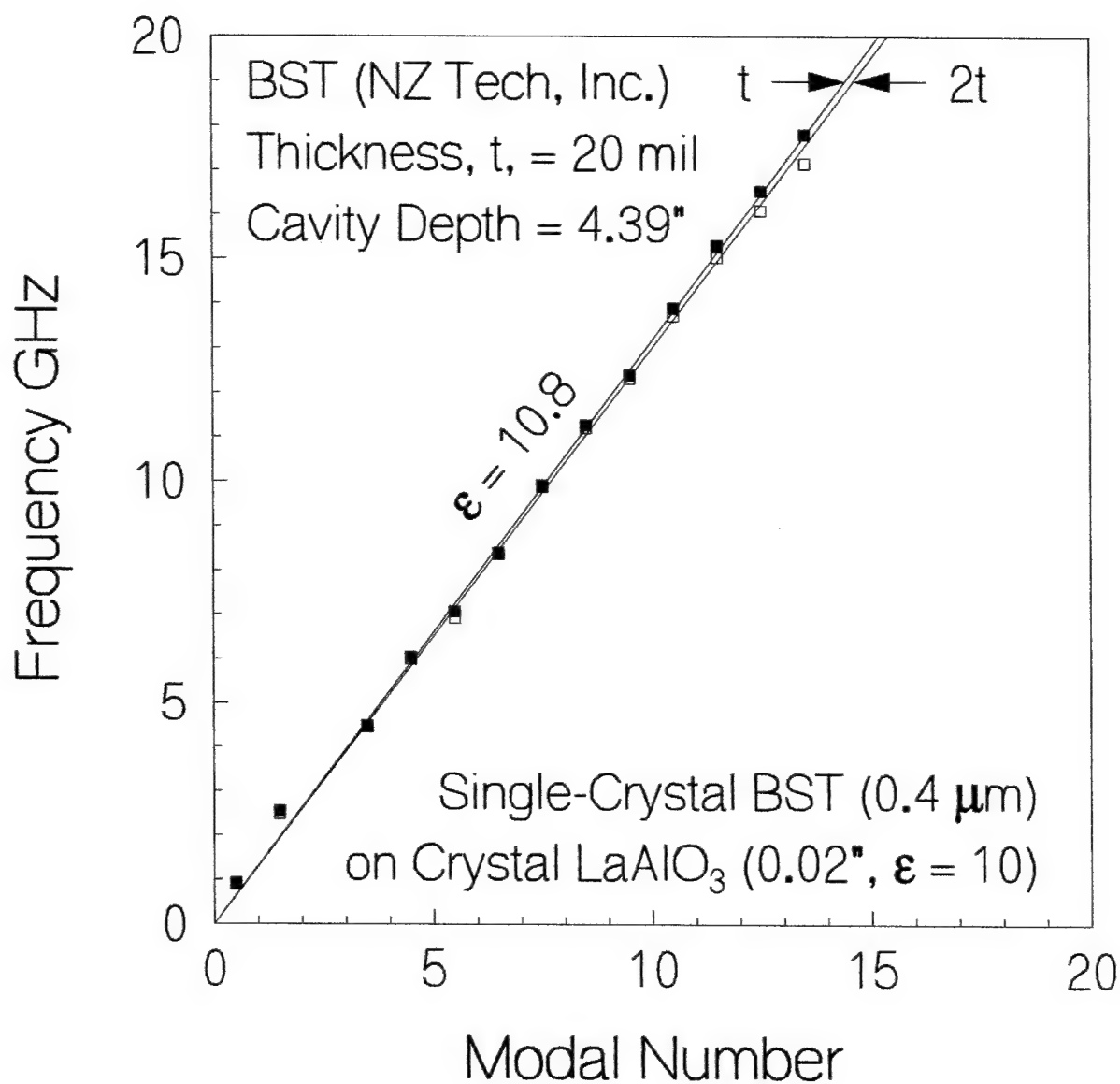
- Modal Spectra Analysis on One/Two Piece(s) of NZ Sample at $V_{bias} = 0$ V
- Full Transmission-Line Analysis Employed
- Perturbation Theory Not Applicable
- Less Electronic Tuning Than Expected
- $\Delta\epsilon/\epsilon \sim +0.1$ at $V_{bias} = 800$ V

# Universal Instrument on Measuring Reflection of TEM-Waves Subject to Electric/Magnetic Bias

Launcher

Collar

7 mm Coax

Insulator
Pin

Central Conductor

Helmholtz
Coil

Sample

Adjustable
Permanent
Bias

Magnet

Bias
Circuit

S11
REF 0.0 dB
5.0 dB/

log MAG

S11
REF 0.0 °
50.0 °/

START   0.045000000 GHz
STOP    18.000000000 GHz

Measurement on G475 Ferrite, 0.15" Thick, Under No Magnetic Bias

- Two Extra Modes Appear in Modal Chart Due to $\lambda/2$ Resonance in Ferrite Sample
- Polarization Degeneracy Removed in $\lambda/2$ Resonance — Left Hand and Right Hand
- $\lambda/2$ Resonance Couples to Linear Resonance in Frequency Interval $\gamma 4\pi M_s$

S11
REF 0.0 dB
5.0 dB/

log MAG

S11
REF 0.0 °
50.0 °/

∠

START    0.045000000  GHz
STOP    18.000000000  GHz

Measurement on G475 Ferrite. 0.15" Thick, Under Permanent Magnet Bias

S11
REF 0.0 dB
5.0 dB/

S11
REF 0.0 °
50.0 °/

log MAG

S11

∠

∠

1→hp
*C
2

V

START   0.045000000  GHz
STOP   18.000000000  GHz

Measurement on G475 Ferrite. 0.15" Thick. Under Magnet and Current Bias

- Near FMR Phase Change Sensitively with the Bias Field and A Small Bias Current can Affect the Reflection Phase Appreciably

Graph axis labels and annotations:
- Y-axis: Change in Modal Frequency (GHz), ranging from -0.6 to 0.6
- X-axis: Frequency (GHz), ranging from 0 to 20

$4\pi M_s = 475$ G

$\Delta H = 200$ Oe,

$\varepsilon = 14.1$

Thich = .15"

L = 4.39"

Permanent Magnet, $H_M$, + Helmholtz Coil, $H_C$

Permanent Magnet Only, $H_M$

$$\bullet \quad \mu_{eff} = \frac{\mu_+ + \mu_-}{2} = 1 + \frac{4\pi M_s H_{in}}{(4\pi M_s)^2 - (f/\gamma)^2}$$

- Calculations Compare Nicely with Experiments
- No Adjustable Parameters Used

S11          log MAG
REF  0.0 °         ∠
      50.0 °/

S11          log MAG
REF  0.0 dB
      5.0 dB/

START    0.045000000 GHz
STOP    18.000000000 GHz

Measurement on G1010 Ferrite, 0.1" Thick, Under No Magnetic Bias

- Two Extra Modes Appear in Modal Chart Due to $\lambda/2$ Resonance in Ferrite Sample
- Polarization Degeneracy Removed in $\lambda/2$ Resonance — Left Hand and Right Hand
- $\lambda/2$ Resonance Couples to Linear Resonance in Frequency Interval $\gamma 4\pi M_s$

S11
REF 0.0 dB
5.0 dB/

log MAG

S11
REF 0.0 °
50.0 °/

S11

∠

START   0.045000000 GHz
STOP   18.000000000 GHz

Measurement on G1010 Ferrite. 0.1" Thick. Under Permanent Magnet Bias

S11
REF 0.0 dB
5.0 dB/

S11
REF 0.0 °
50.0 °/

log MAG

S11

START  0.045000000 GHz
STOP   18.00000000 GHz

Measurement on G1010 Ferrite, 0.1" Thick, Under Magnet and Current Bias

- Near FMR Phase Change Sensitively with the Bias Field and A Small Bias Current can Affect the Reflection Phase Appreciably

$4\pi M_s = 1000$ G
$\Delta H = 200$ Oe,
$\varepsilon = 14.9$
Thich = .1"
L = 4.39"

Permanent Magnet Only, $H_M$

Permanent Magnet, $H_M$, + Helmholtz Coil, $H_C$

Change in Modal Frequncy (GHz)

Frequency (GHz)

- $\mu_{eff} = \dfrac{\mu_+ + \mu_-}{2} = 1 + \dfrac{4\pi M_s H_{in}}{(4\pi M_s)^2 - (f/\gamma)^2}$

- Calculations Compare Nicely with Experiments
- No Adjustable Parameters Used

S11
REF   0.0 °
      50.0 °/

S11
REF   0.0 dB
      5.0 dB/

log MAG

S11
REF   0.0 °

START   0.045000000 GHz
STOP   18.000000000 GHz

Measurement on G1010 Ferrite. 0.15" Thick, Under No Magnetic Bias

- Two Extra Modes Appear in Modal Chart Due to $\lambda/2$ Resonance in Ferrite Sample
- Polarization Degeneracy Removed in $\lambda/2$ Resonance — Left Hand and Right Hand
- $\lambda/2$ Resonance Couples to Linear Resonance in Frequency Interval $\gamma 4\pi M_s$

Measurement on G1010 Ferrite, 0.15" Thick, Under Permanent Magnet Bias

Measurement on G1010 Ferrite, 0.15" Thick, Under Magnet and Current Bias
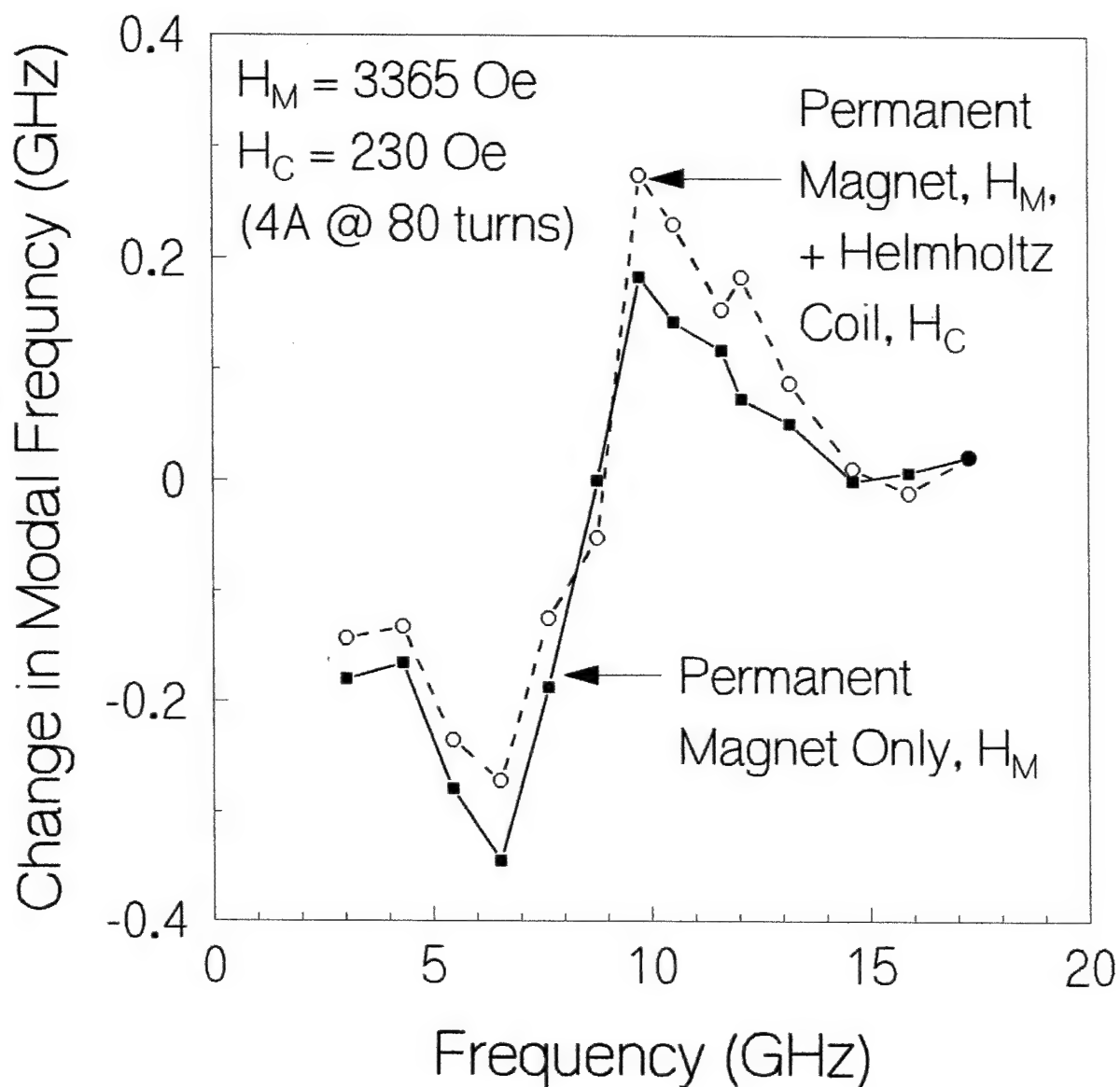
The figure shows "Change in Modal Frequency (GHz)" versus "Frequency (GHz)". Annotations: $H_M$ = 3365 Oe, $H_C$ = 230 Oe (4A @ 80 turns). Curves labeled "Permanent Magnet, $H_M$, + Helmholtz Coil, $H_C$" and "Permanent Magnet Only, $H_M$".

● Near FMR Phase Change Sensitively with the Bias Field and A Small Bias Current can Affect the Reflection Phase Appreciably

The figure shows "Change in Modal Frequency (GHz)" vs "Frequency (GHz)" with parameters:
$4\pi M_s = 1000$ G, $\Delta H = 1000$ Oe, $\varepsilon = 14.9$, Thich = .15", L = 4.39". Curves labeled "Permanent Magnet, $H_M$, + Helmholtz Coil, $H_C$" and "Permanent Magnet Only, $H_M$".
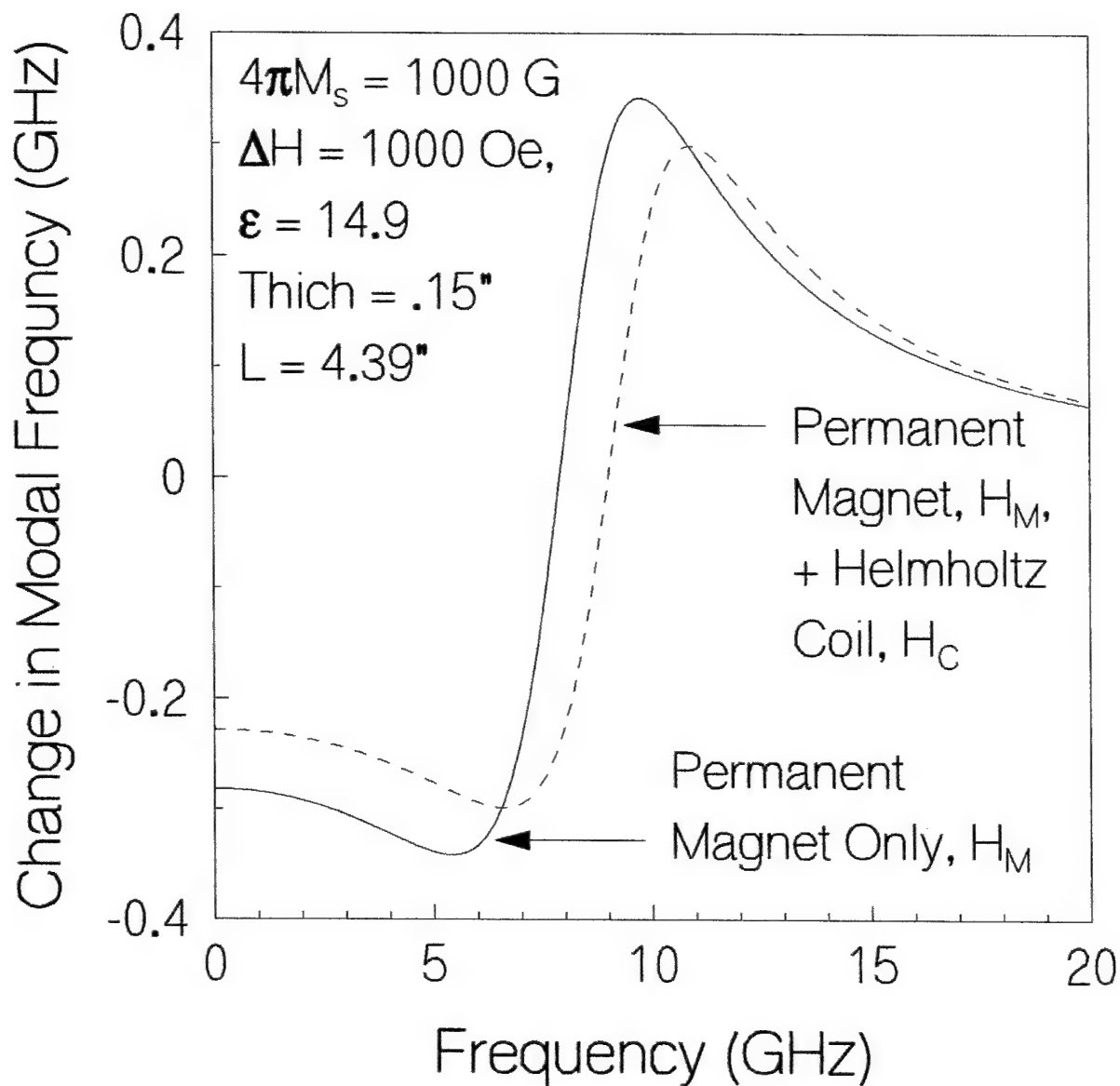
$$\mu_{eff} = \frac{\mu_+ + \mu_-}{2} = 1 + \frac{4\pi M_s H_{in}}{(4\pi M_s)^2 - (f/\gamma)^2}$$

- Calculations Compare Nicely with Experiments
- Due to Bias Inhomogeneity $\Delta H \sim 4\pi M_s$

# Summary

- Local Phase/Impedance adjustment Requires Control in Both $\epsilon$ and $\mu$ via the Application of Voltage and Current

- Application of Ferroelectric and Ferrite

- Grid Electrode Provides Static Electric Bias

- Permanent Magnet Supplies a Bias Magnetic Background

- Resonance mechanisms utilized to enhance tuning sensitivity (FMR + Dimensional Resonance; Lateral and/or Longitudinal)

- Effective experimental instrument fabricated

- Calculations Compared Nicely With Measurements

- Calibration Standards Need to be Fabricated (TRL) to Directly Measure Phase and Impedance Change in Boundary Layer

- Loss Parameters Need to be Addressed

- Simultaneous Control of $\epsilon(E)$ and $\mu(H)$ Over Boundary Layer Need to be Performed

# Calculated and Measured Characteristics of a Microstrip Line Fabricated on a Y-Type Hexaferrite Substrate

Hoton How, Xu Zuo, Elwood Hokanson, Leo C. Kempel, *Senior Member, IEEE*, and Carmine Vittoria, *Fellow, IEEE*

*Abstract*—Numerical calculations have been applied to a microstrip line fabricated on a Y-type hexaferrite substrate using the Green's function technique. The formulation allows the ferrite substrate to be magnetized along an arbitrary direction. Current potentials have been used to construct the Galerkin elements and the resultant calculational scheme is applicable even when ferrimagnetic resonance is approached. Calculations compared reasonably well with measurements.

*Index Terms*—Arbitrary magnetic bias, calculations near ferromagnetic, current-potential method, dyadic Green's function, ferrite substrate, microstrip line, Sommerfeld integral, transfer-matrix method.

## I. INTRODUCTION

ANISOTROPIC substrates, due to either the process in material preparation or crystalline asymmetry, have been used in the fabrication of microwave integrated circuits (MICs). Electromagnetic wave propagation in a ferrite substrate is also anisotropic in the presence of a dc-bias magnetic field, called the gyromagnetic effect. For the former case, the dielectric properties for wave propagation in the substrate can be described in terms of a permittivity tensor of rank 2 and, for the latter case, Polder permeability tensor results under the small-signal approximations [1]. While many authors have applied numerical calculations to microwave circuitries containing anisotropic substrates [2]–[6], in this paper, we consider wave propagation in a gyromagnetic substrate. We specifically consider the electromagnetic wave propagation in a microstrip transmission line in which the metal strip is fabricated on top of a hexaferrite substrate for which the bias magnetic field can be applied along an arbitrary direction. The formulation contained in this paper is applicable to a general stratified dielectric/magnetic structure containing circuit inhomogeneities at the interfaces. A Green's function approach is adopted in the following analysis.

In contrast to the permittivity tensor, Polder tensor elements are usually frequency dependent and exhibit strong resonance behavior with frequency and the bias magnetic field. For example, the effective permeability for wave propagation for frequencies around ferromagnetic resonance (FMR) varies from a very large positive number to a very small negative number encompassing the value zero, accompanied by a nonzero imaginary part accounting for magnetic loss [1]. Most useful magnetic microwave devices operate near FMR so that the rapid change in magnetic permeability can be effectively utilized either to obtain frequency-tuning capability or to remove the degeneracy between modes, thereby inducing nonreciprocity in wave propagation [7]. For example, ferrite phase shifters [8], resonators [9], and filters [1] are constructed according to the first principle [7], and circulators and isolators according to the second [10]. Most calculations in the past have been formulated for frequencies away from FMR in order to avoid numerical difficulties. In this paper, numerical solutions near FMR have been attempted. This was possible for us because we introduced techniques for current potentials to be discussed here.

Before solving the ac electromagnetic problem associated with a ferrite substrate, one is required to solve the dc equilibrium problem first in order to calculate the demagnetizing field due to the finite geometry of the substrate [7]. In a cubic-ferrite sample material, anisotropy is usually not important since it is small in comparison to the external bias field. In a hexaferrite substrate, the internal anisotropy field can be as large as 50 kOe and, hence, it can no longer be neglected [11]. Actually, hexaferrites are purposely introduced to alleviate [12], or even eliminate [13], the external bias field requirement at high frequencies. In a hexaferrite material, magnetic anisotropy appears in the form of an easy axis or an easy plane. For an M-type hexaferrite, the c-axis is an easy axis of magnetization, and the magnetization vector prefers to be aligned along the c-axis so as to lower its free energy [7]. For a Y-type hexaferrite, the ab-plane is an easy plane, and the magnetization vector is energetically favorable to be aligned in the ab-plane [12]. Equations (A14a) and (A14b) describe the respective effective internal fields for an easy axis and an easy plane. In this paper, we consider the substrate material to be a Y-type hexaferrite whose effective field [see (A14b)] is derived elsewhere [12].

For a given geometry, electromagnetic wave solutions arising from a point source satisfying the required (homogeneous) boundary conditions are termed Green's functions [14]. In Section II, we formulate the Green's functions of a general stratified structure containing magnetic and dielectric layers using a transverse spectral-domain analysis. For this purpose,

we need to know *a priori* the plane-wave solutions occurring in each of the layered system. While plane-wave solutions are obvious for an isotropic dielectric layer, plane-wave solutions for an unbounded ferrite bulk magnetized along an arbitrary direction are also well known [1], whose properties are summarized in the Appendix. In general, wave propagation in a magnetized ferrite is nondegenerate, assuming different effective permeability values for different eigenmodes, resulting in different propagation speeds and polarizations.

We have applied the transfer-matrix technique to perform the transverse spectral-domain analysis [2], [6], [15]. A transfer matrix translates the surface impedance, which is itself a $2 \times 2$ matrix, from one layer interface to another, assuming the tangential components of the electromagnetic fields to be continuous across the interfaces in the absence of circuit inhomogeneities. The outermost layers are either air or a metal surface of finite conductivity, defining the (imperfect) open- or short-circuited boundaries for the layered structure, respectively. Thus, via the transfer matrices defined for the layers, these open- and/or short-circuited surface impedances are translated ultimately onto an interface containing a point source assumed by a Green's function and, after imposing the current-continuity condition at the interface position, the corresponding Green's function can, therefore, be solved.

When metal patches or strips appear in the stratified structure, as required by a microwave circuit, electromagnetic solutions can be constructed via superposition of the Green's functions. That is, electromagnetic solutions are cast in integral forms where Green's functions are superposed according to an unknown source distribution. The unknown source distribution can then be solved numerically using the Galerkin's method applied to an integral equation expressing the condition for current continuity [16]. We have used current potentials to construct the Galerkin elements and by doing so three advantages follow [17]. Not only is the symmetry of the patch/strip conserved in the calculations, but the vector Galerkin equations are also converted into scalar ones, resulting in onefold integrals for the one-dimensional (1-D) transmission-line problems and twofold integrals for the two-dimensional (2-D) metal-patch problems. Most importantly, the condition for current continuity at metal-patch/strip boundaries is automatically satisfied, forcing the normal components of the current flow to vanish at the boundaries of the metal patches/strips [18]. By using the current-potential techniques, we are able to apply numerical calculations to microstrip circuitries containing ferrite substrates even when FMR is approached. When FMR is approached, the underlying numerical problem becomes ill defined and the Galerkin elements need to be scaled to avoid large truncation errors.

As just mentioned, the resultant Galerkin elements associated with a transmission-line problem require evaluation of onefold Sommerfeld-type integrals. However, due to the fixed period $(2\pi)$ of the sine and cosine functions, numerical integration at infinity is less stringent than the original Sommerfeld-type integrals containing oscillations of Bessel functions at infinity [16]. As such, extrapolation schemes have been applied to evaluate the integrals at infinity.
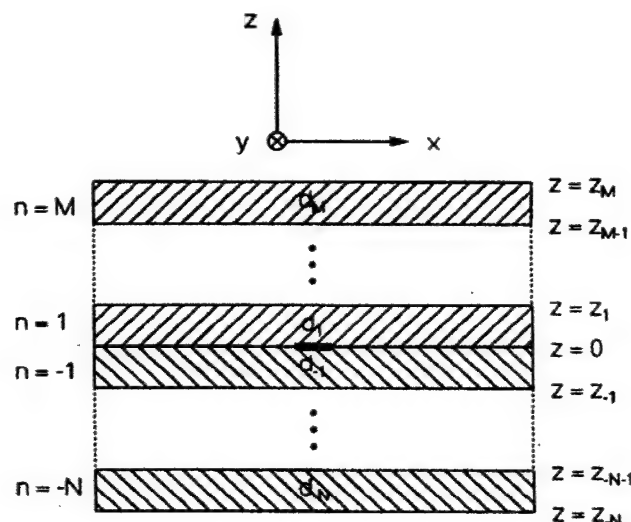


Fig. 1. Geometry of a stratified structure containing multiple layers. A planar circuit is located at the $z = 0$ plane.

Experimentally, we have fabricated a microstrip transmission line on a Y-type hexaferrite substrate exhibiting a magnetic easy plane [12]. While the significance of a magnetic easy plane is discussed in a separate paper [12], numerical calculations for wave propagation along a microstrip line involving a magnetic easy plane implied by a Y-type hexaferrite substrate follow in this paper. Calculations compared reasonably well with measurements.

## II. FORMULATION

We present a general formulation that a planar microwave circuit is embedded in a stratified structure involving dielectric/magnetic layers as substrates/superstrates. This is shown in Fig. 1. The planar circuit is located at $z = 0$ and there are $M$ layers in the $+z$-direction and $N$ layers in the $-z$-direction. We denote $z$ as the direction normal to the layered structure. The thickness of the $\nu$th layer is $d_\nu$, $M \geq \nu \geq -N$. In Fig. 1, the outermost surfaces are either a metal boundary of finite conductivity $\sigma$ or air. The following formulation allows the boundary conditions at the outermost surfaces $z = z_M$ and $z = z_{-N}$ to be translated onto the interface at $z = 0$ containing the microwave circuit, admitting a 2-D analysis there. For this purpose, we have adopted the so-called transfer-matrix technique [2], [6], [15]. Although the present analysis considers only one single plane that contains the circuit inhomogeneity, the same analysis can be generalized so that more than one planar circuits may appear at several layer interfaces. In Fig. 1, the resultant electromagnetic wave solutions in the presence of a vertical point dipole is termed as the dyadic Green's function [16].

The transfer-matrix method is applied in the spectral domain. A transfer matrix is a $4 \times 4$ matrix and, for a given transverse spectral vector $\underline{k}_t = (k_x \ k_y)^T$, it correlates the tangential components of the RF $e$- and $h$-fields on both sides of a layer [see (3)]. Here, the superscript $T$ denotes transposition of a row

vector into a column vector. Thus, for the $\nu$th layer the transfer matrix can be written as

$$\underline{\underline{T}}_\nu(d_\nu) = \underline{\underline{\Gamma}}_\nu(z_{\nu+1}) \cdot \underline{\underline{\Gamma}}_\nu^{-1}(z_\nu) \tag{1}$$

with (2), shown at the bottom of this page, so that

$$\begin{pmatrix} e_x(z_{\nu+1}) \\ e_y(z_{\nu+1}) \\ h_x(z_{\nu+1}) \\ h_y(z_{\nu+1}) \end{pmatrix} = \underline{\underline{T}}_\nu(d_\nu) \cdot \begin{pmatrix} e_x(z_\nu) \\ e_y(z_\nu) \\ h_x(z_\nu) \\ h_y(z_\nu) \end{pmatrix}. \tag{3}$$

In (2), $k_{\nu\alpha z}$, $M \geq \nu \geq -N$, and $4 \geq \alpha \geq 1$ denotes the $z$-component of the wave vector of the $\alpha$th eigenmode in the $\nu$th layer satisfying

$$k_x^2 + k_y^2 + k_{\nu\alpha z}^2 = \epsilon_{\nu\alpha}\mu_{\nu\alpha}(\omega/c)^2. \tag{4}$$

In (4), $\epsilon_{\nu\alpha}$ and $\mu_{\nu\alpha}$ are the dielectric constant and permeability of the $\alpha$th eigenmode in the $\nu$th layer, $\omega$ is the angular frequency, $c$ the speed of light in vacuum, and Gaussian units have been used throughout this analysis.

For an isotropic medium, (4) reduces to the regular dispersion relation for wave propagation, and $\epsilon_{\nu\alpha}$ and $\mu_{\nu\alpha}$ are all degenerate, i.e., $\alpha$ independent, denoting the permittivity and permeability of the medium, respectively. For an anisotropic medium, the four eigenmodes become nondegenerate, assuming different values for permittivity and/or for permeability $\epsilon_{\nu\alpha}$ and $\mu_{\nu\alpha}$, $\alpha = 1, 2, 3, 4$. The procedure for solving the nondegenerate dispersion relation of a gyromagnetic medium is given in the Appendix. That is, when $k_x$, and $k_y$ are given, $k_{\nu\alpha z}$ is solved from (A5). Since (A5) is a quartic equation, there are four eigenmodes, corresponding to the four solutions of $k_{\nu\alpha z}$. Equation (4) then solves for $\mu_{\nu\alpha}$, denoting the effective permeability of the $\alpha$th mode, which is used to express the electromagnetic fields of the $\alpha$th eigenmode given in (A20)–(A28). The permittivity of the eigenmodes are all the same, $\epsilon_{\nu\alpha} = \epsilon_d, \alpha = 1, 2, 3, 4$, where $\epsilon_d$ denotes the dielectric constant of the ferrite layer. More details about the solution of the eigenmodes can be found in the Appendix as related to (A5).

We note in the limit of a transversely applied magnetic bias field the coefficients $P_3 = P_1 = 0$ [see (A7) and (A8)] since $e_{nz} = 0$. Thus, (A5) implies two doubly degenerate eigenmode pairs, as derived in [6]. It can be shown that (A5) reduces to the corresponding equations in [6] for a transversely applied bias field. However, if the bias field is along an arbitrary direction, (A5) predicts, in general, four nondegenerate eigenmodes. We note that FMR occurs if the coefficient $P_4 = 0$ [see (A6)]. At FMR, (A5) implies an incomplete set of eigenmodes, which spans a vector space with dimensionality smaller than required

by the present spectral-domain analysis or the transfer matrix techniques [see (1)].

The tangential components of the $e$ and $h$-fields associated with the $\alpha$th eigenmode in the $\nu$th layer are expressed as $(e_{\nu\alpha x} \; e_{\nu\alpha y})^T$ and $(h_{\nu\alpha x} \; h_{\nu\alpha y})^T$ in (2), respectively. The $\Gamma$-matrices and, hence, the transfer matrices $\underline{\underline{T}}_\nu(d_\nu)$ for a dielectric layer and for a ferrite layer [see (2)] are given in the Appendix. The index $\nu$ has been dropped in the Appendix for reasons of clarity.

The surface impedance matrix $\underline{\underline{Z}}(z)$ can be defined as follows:

$$\begin{pmatrix} e_x(z) \\ e_y(z) \end{pmatrix} = \underline{\underline{Z}}(z) \cdot \begin{pmatrix} h_x(z) \\ h_y(z) \end{pmatrix} \tag{5}$$

where the dependence of the quantities in (5), say, $e_x$, $e_y$, $h_x$, $h_y$, and $\underline{\underline{Z}}$ on $k_x$ and $k_y$ is understood. Thus, when a transfer matrix is defined to translate the tangential components of the RF electromagnetic fields over one layer thickness [see (3)], the surface impedance will also be transferred according to the following equation:

$$\underline{\underline{Z}}(z_{\nu+1}) = \left[ \underline{\underline{a}}_\nu \underline{\underline{Z}}(z_\nu) + \underline{\underline{b}}_\nu \right] \left[ \underline{\underline{c}}_\nu \underline{\underline{Z}}(z_\nu) + \underline{\underline{d}}_\nu \right]^{-1} \tag{6}$$

where $\underline{\underline{a}}_\nu$, $\underline{\underline{b}}_\nu$, $\underline{\underline{c}}_\nu$, and $\underline{\underline{d}}_\nu$ are the $2 \times 2$ partition matrices of $\underline{\underline{T}}_\nu$ given by

$$\underline{\underline{T}}_\nu = \begin{pmatrix} \underline{\underline{a}}_\nu & \underline{\underline{b}}_\nu \\ \underline{\underline{c}}_\nu & \underline{\underline{d}}_\nu \end{pmatrix}. \tag{7}$$

Since, except at $z = 0$, the tangential components of the $e$- and $h$-fields are continuous across layer interfaces, the transfer matrices can be multiplied together to provide an overall transformation relating the outermost boundaries of the structure to the $z = 0$ plane. Thus, we define two overall transfer matrices, top and bottom, denoted as $\underline{\underline{T}}_t$ and $\underline{\underline{T}}_b$, respectively, as

$$\underline{\underline{T}}_t = \left[ \underline{\underline{T}}_M \cdots \underline{\underline{T}}_2 \underline{\underline{T}}_1 \right]^{-1} \tag{8}$$

$$\underline{\underline{T}}_b = \underline{\underline{T}}_{-N} \cdots \underline{\underline{T}}_{-2} \underline{\underline{T}}_{-1} \tag{9}$$

such that

$$\begin{pmatrix} e_x(0^+) \\ e_y(0^+) \\ h_x(0^+) \\ h_y(0^+) \end{pmatrix} = \underline{\underline{T}}_t \cdot \begin{pmatrix} e_x(z_M) \\ e_y(z_M) \\ h_x(z_M) \\ h_y(z_M) \end{pmatrix}$$

$$\begin{pmatrix} e_x(0^-) \\ e_y(0^-) \\ h_x(0^-) \\ h_y(0^-) \end{pmatrix} = \underline{\underline{T}}_b \cdot \begin{pmatrix} e_x(z_{-N}) \\ e_y(z_{-N}) \\ h_x(z_{-N}) \\ h_y(z_{-N}) \end{pmatrix}. \tag{10}$$

$$\underline{\underline{\Gamma}}_\nu(z) = \begin{pmatrix} e_{\nu 1x}\exp(ik_{\nu 1z}z) & e_{\nu 2x}\exp(ik_{\nu 2z}z) & e_{\nu 3x}\exp(ik_{\nu 3z}z) & e_{\nu 4x}\exp(ik_{\nu 4z}z) \\ e_{\nu 1y}\exp(ik_{\nu 1z}z) & e_{\nu 2y}\exp(ik_{\nu 2z}z) & e_{\nu 3y}\exp(ik_{\nu 3z}z) & e_{\nu 4y}\exp(ik_{\nu 4z}z) \\ h_{\nu 1x}\exp(ik_{\nu 1z}z) & h_{\nu 2x}\exp(ik_{\nu 2z}z) & h_{\nu 3x}\exp(ik_{\nu 3z}z) & h_{\nu 4x}\exp(ik_{\nu 4z}z) \\ h_{\nu 1y}\exp(ik_{\nu 1z}z) & h_{\nu 2y}\exp(ik_{\nu 2z}z) & h_{\nu 3y}\exp(ik_{\nu 3z}z) & h_{\nu 4y}\exp(ik_{\nu 4z}z) \end{pmatrix} \tag{2}$$

The relationship between the two column vectors $(e_x(0^+)e_y(0^+)h_x(0^+)h_y(0^+))^T$ and $(e_x(0^-)e_y(0^-)h_x(0^-)h_y(0^-))^T$ is determined from the boundary conditions imposed by the planar circuit at $z = 0$, as connected together by the use of the dyadic Green's functions discussed below. We note that while transfer matrices are multiplied together translating the tangential components of the electromagnetic fields across layers, as described by (8) and (9), the transformation of surface impedance defined by the functional form of (6) also multiplies or compounds as a consequence of the translation process. This is indeed true since transformation of (6) is an isomorphic representation of the transfer matrix $\underline{\underline{T}}_\nu$ under the operation of matrix multiplication. Therefore, we have

$$\underline{\underline{Z}}(0^+) = \left[\underline{\underline{a}}_t\underline{\underline{Z}}(z_M) + \underline{\underline{b}}_t\right]\left[\underline{\underline{c}}_t\underline{\underline{Z}}(z_M) + \underline{\underline{d}}_t\right]^{-1} \quad (11)$$

$$\underline{\underline{Z}}(0^-) = \left[\underline{\underline{a}}_b\underline{\underline{Z}}(z_{-N}) + \underline{\underline{b}}_b\right]\left[\underline{\underline{c}}_b\underline{\underline{Z}}(z_{-N}) + \underline{\underline{d}}_b\right]^{-1} \quad (12)$$

where $\underline{\underline{a}}_t$, $\underline{\underline{b}}_t$, $\underline{\underline{c}}_t$, and $\underline{\underline{d}}_t$ denote the partition matrices associated with the top transfer matrix, e.g., $\underline{\underline{T}}_t$.

Now we need to know the surface impedance of the outermost surfaces. We consider the surface impedances $\underline{Z}(z_M)$ and $\underline{Z}(z_{-N})$ to be those associated with either a short-circuited metal ground plane or an open-circuited half-space filled with, say, air. For a short-circuited ground plane, the surface impedance can be derived as

$$\underline{\underline{Z}}_s = \pm\left[\frac{c}{4\pi}\right]\frac{1-i}{\sigma\delta}\begin{pmatrix} 0 & 1 \\ -1 & 0 \end{pmatrix} \quad (13)$$

and for an open-circuited half-space

$$\underline{\underline{Z}}_o = \pm\begin{pmatrix} e_{Ax} & e_{Bx} \\ e_{Ay} & e_{By} \end{pmatrix}\begin{pmatrix} 0 & \sqrt{\frac{\mu_o}{\epsilon_o}} \\ -\sqrt{\frac{\mu_o}{\epsilon_o}} & 0 \end{pmatrix}\begin{pmatrix} e_{Ax} & e_{Bx} \\ e_{Ay} & e_{By} \end{pmatrix}^{-1} \quad (14)$$

where the $+(-)$ sign applies if the surface being considered possesses an upward (downward) surface normal. In (13), $\sigma$ denotes the electrical conductivity of the metal plane, and $\delta = c(2\pi\omega\sigma)^{-1/2}$ is the skin depth. In (14), $\epsilon_o$ and $\mu_o$ are the dielectric constant and magnetic permeability of the open space, which may differ from one if material other than air is used in filling the half-space. The column vectors $\underline{e}_A = (e_{Ax}\ e_{Ay})^T$ and $\underline{e}_B = (e_{Bx}\ e_{By})^T$ are defined in (A1) and (A2). Thus, once the surface impedances $\underline{Z}(z_M)$ and $\underline{Z}(z_{-N})$ are given from (13) or (14), $\underline{Z}(0^+)$ and $\underline{Z}(0^-)$ can then be calculated from (11) and (12) provided that all of the transfer matrices $\underline{\underline{T}}_\nu$, $M \geq \nu \geq -N$ are known a priori [see (7) and (8)]. Note that the present formulation encompasses losses of all kinds, including dielectric loss [see (A4) and (A15)], magnetic loss [see (A14a) and (A14b)], and conductor loss [see (13) and (17)]; radiation-wave loss presents in (14) and surface-wave loss is inherent to the Green's function construction contained in the transfer matrices $\underline{\underline{T}}_t$ and $\underline{\underline{T}}_b$ [see (8) and (9)].

Let $\underline{G}(k_x, k_y)$ be the Green's function dyad in the spectral domain denoting the tangential electric field generated by a point-dipole source located at the $z = 0$ interface. That is, for a given current distribution in the interface $\underline{j}(x', y')$, the generated tangential electric field at $z = 0$ is

$$\underline{e}_t(x, y) = \frac{1}{4\pi^2}\int_{-\infty}^{\infty} dk_x \int_{-\infty}^{\infty} dk_y \int_{-\infty}^{\infty} dx' \int_{-\infty}^{\infty} dy'$$
$$\cdot \exp\left[ik_x(x - x')\right]\exp\left[ik_y(y - y')\right]$$
$$\cdot \underline{G}(k_x, k_y)\underline{j}(x', y'). \quad (15)$$

From Ampere's law, the Green's function dyad is

$$\underline{G}(k_x, k_y) = \left\{\left[\underline{\underline{Z}}(0^+; k_x, k_y)\right]^{-1} - \left[\underline{\underline{Z}}(0^-; k_x, k_y)\right]^{-1}\right\}^{-1}$$
$$\cdot \begin{pmatrix} 0 & 1 \\ -1 & 0 \end{pmatrix}. \quad (16)$$

In (15), both the source point $(x'\ y')$ and the observation point $(x\ y)$ are located at $z = 0$. The integral equation to solve is [16], [17]

$$\underline{e}_t(x, y) + Z_s\underline{j}(x, y) = \underline{E}_c(x, y) \quad (17)$$

where

$$Z_s = (1 - i)(\omega/8\pi\sigma)^{1/2} \quad (18)$$

denotes the surface impedance, $\sigma$ denotes the conductivity of the metal patch at $z = 0$, and $\underline{E}_c$ denotes the tangential component of the electric field generated by the excitation current or the feeder-line current.

In this paper, we consider the microstrip solutions for which wave propagates along the $y$-direction without imposing to external-current excitation $\underline{E}_c = 0$ in (17). That is, we are considering the normal-mode solutions intrinsic to a microstrip transmission line. Under these considerations, (15) and (17) are combined to yield

$$\frac{1}{2\pi}\int_{-\infty}^{\infty} dk \int_{-\infty}^{\infty} dx' \exp\left[ik(x - x')\right]\underline{G}(k, \beta)\underline{j}(x')$$
$$- Z_s\underline{j}(x) = 0. \quad (19)$$

Here, for clarity, we have used different symbols $k$ and $\beta$ for $k_x$ and $k_y$, respectively. The homogeneous equations [i.e., (19)] are then solved numerically, giving rise to the dispersion relation expressing the wave propagation constant $\beta$ as a function of the angular velocity $\omega$.

The microstrip geometry is depicted in Fig. 2, where the metal strip is of width $w$, lying on the $z = 0$ plane, extending from $x = 0$ to $x = w$. Following [16] and [17], we express the current distribution in the metal strip in terms of a current basis $\{\underline{j}_m\}$

$$\underline{j}(x, y) = \sum_{m=0}^{\infty} a_m\underline{j}_m(x, y) \quad (20)$$

where the current elements $\{\underline{j}_m\}$ are derived from current potentials as

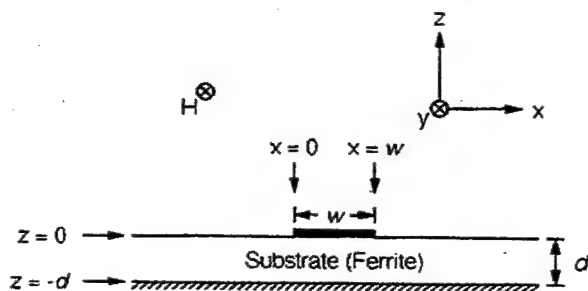$$\underline{j}_m(x, y) = \underline{\nabla}_t\left[\cos(m\pi x/w)e^{i\beta y}\right], \qquad m = 0, 1, 2, \ldots. \quad (21)$$

Fig. 2. Geometry of the microstrip line fabricated on a Y-type hexaferrite substrate.

Here, $\underline{\nabla}_t$ denotes the two-dimensional transverse gradient operator. Note that the normal components of the current elements vanish at the microstrip edges, as required by the current continuity equation [18]. By using the Galerkin's method the Galerkin elements associated with (19) are

$$
\begin{aligned}
A_{mn} &= \frac{1}{2\pi} \int_{-\infty}^{\infty} dk \int_0^w dx \int_0^w dx' e^{ik(x-x')} \underline{j}_m(x')^+ \\
&\quad \cdot \underline{G}(k,\beta)\underline{j}_n(x) + Z_s \int_0^w dx \underline{j}_m(x)^+ \underline{j}_n(x) \\
&= \frac{1}{2\pi} \int_{-\infty}^{\infty} dk \left\{ \left(\frac{m\pi}{w}\right)^2 \left(\frac{n\pi}{w}\right)^2 G_{11} \right. \\
&\quad + \beta k \left[ \left(\frac{m\pi}{w}\right)^2 G_{12} + \left(\frac{n\pi}{w}\right) G_{21} \right] \\
&\quad \left. + \beta^2 k^2 G_{22} \right\} \\
&\quad \cdot \frac{\left[ e^{i(kw+m\pi)} + 1 \right] \left[ -e^{-i(kw+n\pi)} + 1 \right]}{\left[ k^2 - (m\pi/w)^2 \right] \left[ k^2 - (n\pi/w)^2 \right]} \\
&\quad + \delta_{mn} \frac{w}{2} \left[ \left(\frac{m\pi}{w}\right)^2 + \beta^2 \right] Z_s
\end{aligned}
\tag{22}
$$

where $\delta_{mn}$ denotes the delta–Kronecker function and the dagger + denotes adjoint operation. By setting the determinant of the Galerkin matrix $(A_{mn})$ into 0, the dispersion relation for wave propagation is determined, expressing the propagation constant $\beta$ as a function of the angular velocity $\omega$. In calculating the Galerkin elements, twofold integrations have been carried out analytically and it is only required to evaluate a onefold integration numerically [see (22)].

By employing the current potentials, the Galerkin equation has been reduced from vector form (19) to scalar form (22). Symmetry retains in the calculations for Galerkin elements. For example, in isotropic media, the left–right symmetry of the microstrip geometry implies that we need only to evaluate even-numbered elements, i.e., $m$ and $n$ are even numbers in (22). Also, integration for $k$ from $-\infty$ to 0 in (22) is the same as from 0 to $\infty$ since wave propagation is reciprocal due to the mirror symmetry of the circuit. However, in an anisotropic medium, say, a ferrite, the presence of a bias magnetic field removes these symmetries. As a result, microstrip currents are shifted onto one side of the metal strip, known as the field displacement effect in the literature [1]. Wave propagation becomes nonreciprocal since the mirror symmetry no longer holds due to the presence of the bias magnetic field or the anisotropy field.

## III. RESULTS

Similar to the original Sommerfeld integrals, surface modes appear, due to poles in the integrand of (22). We note that the lateral strip-resonant modes, occurring at $k = \pm m\pi$ and $\pm n\pi$, are actually not poles of the integrand since, at these wave numbers, the numerator of the integrand also vanishes, appearing as first-order zeros. The same results occur for other metal patch geometries, as illustrated in [16] and [17]. Numerical techniques evaluating Sommerfeld-type integrals are discussed in [16] and [17], and most techniques still apply here. However, due to the fixed period of the integrand at infinity, say, $2\pi$, integration of these integrands can be carried out using an extrapolation scheme.

Due to losses of various kinds, surface poles are pushed off from the real $k$-axis, allowing the integrals to be evaluated numerically. However, sharp cancellation occurs near surface poles and the integration processes need to be handled with care [16], [17]. In performing numerical integrations, we define a cutoff for the wavenumber $k$. Integration from $-$cutoff to $+$cutoff is accomplished using the implicit fifth-order Runge–Kutta method, which is able to monitor local truncation errors to adaptively adjust step size to ensure the overall integration accuracy [19]. Integrations from $-\infty$ to $-$cutoff and from cutoff to $\infty$ are then evaluated using the extrapolation scheme. Initial value for cutoff is set to be $100 \, (\omega/c)\epsilon_f^{1/2}$. This cutoff value is then doubled to check the overall accuracy. This process continues until the required tolerance is met.

Calculations of Galerkin elements have been carried out retaining six significant digits when outside the FMR region. When FMR is approached, the Galerkin matrix becomes ill behaved. We have to scale the matrix elements properly to avoid numerical underflow and to avoid large truncation errors. FMR region is defined for $\omega_K < \omega < \omega_{FMAR}$, and $\omega_K$ and $\omega_{FMAR}$ are the Kittel frequency and ferromagnetic antiresonant frequency given by [12, eqs. (7) and (8)], respectively. In the following calculations, we have used 20 Galerkin elements. Once the wavenumber $\beta$ is solved as the lowest zero of the eigenvalues, the fundamental mode, the unknown current expansion coefficient $a_m$, $m = 0, 1, 2, 3, \ldots$ [see (20)] are determined as the associated eigenvector.

Impedance of a transmission line supporting TEM-like wave propagation can be defined as

$$
Z_L = V/I
\tag{23}
$$

where $V$ is the voltage drop across the central conductor and ground plane and $I$ is the current flowing at the central conductor. For the microstrip line shown in Fig. 2, $I$ can be calculated as

$$
I = \int_0^w dx j_Y = i\beta a_0
\tag{24}
$$

and $V$ can be calculated from

$$
V = \frac{1}{2\pi} \int_{-\infty}^{\infty} dk \int_0^w dx' \int_w^{\infty} dx e^{ik(x-x')} \begin{pmatrix} 1 \\ 0 \end{pmatrix}^T \cdot \underline{G}(k,\beta)\underline{j}_m(x').
\tag{25}
$$

From (23), we obtain

$$Z_L = \frac{1}{2\pi\beta} \sum_{m=0}^{\infty} \left(\frac{a_m}{a_0}\right) \int_{-\infty}^{\infty} dk \frac{e^{ikw}}{k} \left[ \left(\frac{m\pi}{w}\right)^2 G_{11} + \beta k G_{12} \right]$$
$$\cdot \frac{1 - e^{-i(kw - m\pi)}}{k^2 - (m\pi/w)^2}. \quad (26)$$

In (25), in calculating the voltage drop, we have chosen the integration path to be along $w < x < \infty$ and $z = 0$. As can be verified from Faraday's law, this voltage drop is independent of the integration path connecting the central conductor with the ground plane so long as the longitudinal component of the RF $h$-field is negligible comparing to the transverse components, i.e., $h_y \ll h_x$ or $h_z$. Otherwise, the concept of line impedance does not make much sense. Here, we also assume the strip is made of good conductor so that voltage drop across the metal strip is negligible. It can be proven that, for a transmission line supporting TEM-like waves, the definition for line impedance [see (23)] is equivalent to

$$Z_L = 2P/I^*I \quad (27)$$

where $P$ is the power delivered by the transmission line.

Under transmission measurement, a transmission line of length $\ell$, impedance $Z_L$, and wave propagation constant $\beta$ is connected with probes at two ends of standard impedance $Z_o = 50\,\Omega$, or $Z_o = 4\pi/c$, which is expressed in Gaussian unit. The transmission coefficient is

$$\tau = \frac{2Z_o Z_L}{2Z_o Z_L \cos\beta L - i\left(Z_o^2 + Z_L^2\right)\sin\beta L} \quad (28)$$

and the reflection coefficient is

$$\rho = \frac{-i\left(Z_O^2 - Z_L^2\right)\sin\beta L}{2Z_o Z_L \cos\beta L - i\left(Z_o^2 + Z_L^2\right)\sin\beta L}. \quad (29)$$

Experimentally, we have fabricated a microstrip transmission line using a single-crystal Y-type hexaferrite as the substrate material [12]. The composition of the substrate material is $Ba_2MgZnFe_{12}O_{22}$ and the easy plane coincides with the substrate surfaces, i.e., the $xy$-plane. The hexaferrite substrate material was characterized using a vibrating sample magnetometer (VSM) to show a saturation magnetization $4\pi M_S = 2.86$ kg, and an anisotropy field $H_A = 7.94$ kOe. The fabricated microstrip line is characterized by the following parameters: thickness $d = 0.010$ in, width $w = 0.0051$ in, length $\ell = 4$ mm, and dielectric constant $\epsilon_f = 18$. The dielectric loss tangent $\tan\delta_f$ was assumed to be 0.01 and FMR linewidth $\Delta H = 100$ Oe. Other properties of the fabricated microstrip line, as well as measurements, can be found in [12].

Fig. 3 shows the calculated current profile of the longitudinal current $j_y(x)$ and the transverse current $j_x(x)$ plotted over the width of the metal strip, assuming the external field $H_o = 5$ kOe, and the frequency $f = 20$ GHz. It is seen in Fig. 3 that current distribution is slightly asymmetric with respect to the center of the strip, showing the field displacement effect due to the presence of a bias magnetic field. Longitudinal currents are crowded at the edges of the strip at which positions the transverse current vanishes, as expected.
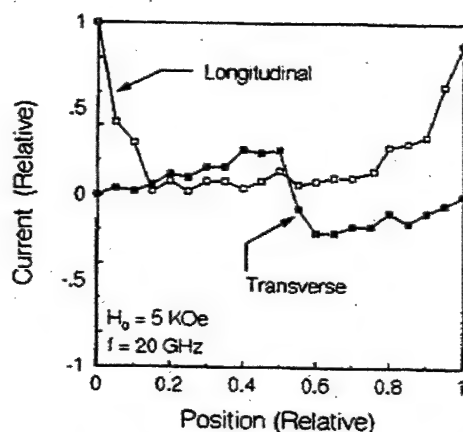


Fig. 3. Calculated current profile for the longitudinal and transverse components across the strip width of the fabricated microstrip line.
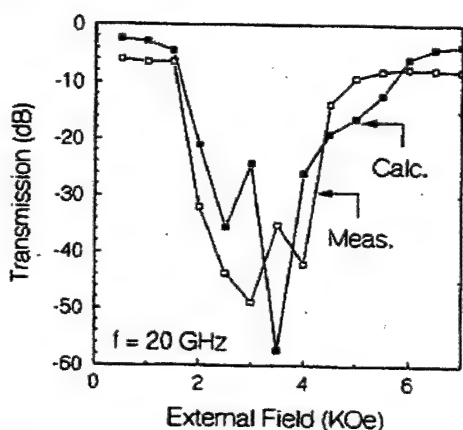


Fig. 4. Calculated and measured transmission amplitude at 20 GHz, plotted as a function of the external bias field.
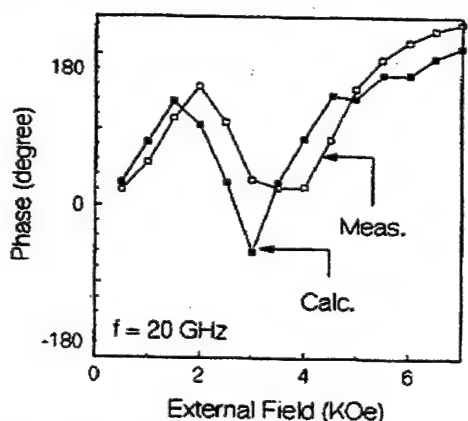


Fig. 5. Calculated and measured transmission phase at 20 GHz, plotted as a function of the external bias field.

Figs. 4 and 5 plot the calculated and measured transmission coefficient for the amplitude and phase, respectively, assuming the frequency $f = 20$ GHz. In Fig. 4, the measured insertion loss is larger than calculated even outside the FMR region. Reasons for this may be that the dielectric loss tangent and FMR linewidth assumed by the calculations are smaller than their actual values, corresponding to electric and magnetic losses, respectively. Other losses, for example, discontinuity resulted

from the coax-microstrip adapters employed under transmission measurements, may also partially explain the discrepancy. Discrepancy between theory and calculations in the FMR region is even bigger due to the difficulty in obtaining good numerical accuracy in that region. Also, the impedance value calculated by using (26) may not be adequate in the FMR region since, to large extent, wave propagation is no more TM-like. Measurements show that wave propagation in the fabricated microstrip line is roughly reciprocal, especially when outside the FMR region.

The calculated transmission phase basically confirms measurements (Fig. 5) showing a resonant structure when FMR comes across. Of special notice, it is seen in Fig. 5 that phase shift occurs linearly in the low field region prior to FMR, suggesting that a transmission line involving Y-type hexaferrite material is a superior candidate for phase shifters, especially at high frequencies. For a Y-type hexaferrite material, the crystalline anisotropy can be effectively used to substitute, at least partially, the bias field requirement. For example, in the absence of a material anisotropy, an external field in the order of 7 kOe is required to effectively change the phase of a microwave signal at 20 GHz. Similarly, an M-type hexaferrite can also provide an internal field along the easy axis, thereby alleviating the bias field requirement. However, in using an M-type hexaferrite, it is inevitable to introduce a demagnetizing field in the order of $4\pi M_s$ [see (A14a)] and, hence, it is not favorable for practical applications, at least as phase shifters. M-type hexaferrite have been practically used to fabricate self-biased circulators at millimeter-wave frequencies [7].

## IV. CONCLUSIONS

We conclude that Green's function calculations utilizing the current-potential technique provide sufficient accuracy in calculating a layered structure containing anisotropic ferrite substrates/superstrates magnetized along an arbitrary direction. Our calculations are applicable even when the region of FMR is approached. The formulation may be generalized to include circuit inhomogeneities at multiple interfaces. For a transmission-line like geometry, the calculations are 1-D, and for a antenna-patch-like geometry the calculations are 2-D. However, if the finite lateral dimension is considered important, one needs to revert to a full-wave three-dimensional (3-D) analysis invoking generic numerical routines for finite-element and finite-difference calculations. The fit between our calculated and measured phase shift and amplitude as a function of the bias field is reasonable in view of the fact that there were no adjustable parameters. All parameters used in the calculations were obtained directly from measurements, including dc, VSM, and FMR measurements [12].

## APPENDIX

For clarity, the layer index $\nu$ is dropped in the following discussion. For an isotropic dielectric medium, the four eigenmodes are degenerate so that $\epsilon_1 = \epsilon_2 = \epsilon_3 = \epsilon_4 = \epsilon_d$ and $\mu_1 = \mu_2 = \mu_3 = \mu_4 = 1$. Here, $\epsilon_d$ denotes the dielectric constant of the medium. The longitudinal wave propagation constant $k_z$ can thus be calculated from (4) for $\alpha = 1, 2, 3$, and 4. Denote the azimuthal and polar angles of the column vector $\underline{k} = (k_x \ k_y \ k_z)^T$ as $\phi$ and $\theta$, respectively. We define two column vectors

$$\underline{e}_A = (1 - (1 - \cos\theta)\cos^2\phi - (1 - \cos\theta)\sin\phi\cos\phi)^T \quad (A1)$$

$$\underline{e}_B = (-(1 - \cos\theta)\sin\phi\cos\phi 1 - (1 - \cos\theta)\sin^2\phi)^T \quad (A2)$$

from which the $\Gamma$-matrix [see (2)] can be written as shown in (A3) at the bottom of this page. In (A3), we have defined the wave impedance of the medium as $\zeta = \epsilon_d^{-1/2}$. In order to take into account dielectric loss, the dielectric constant $\epsilon_d$ shall be replaced by a complex number whose imaginary part is proportional to the dielectric loss tangent of the medium $\tan\delta_d$

$$\epsilon_d \to \epsilon_d(1 + i\tan\delta_d). \quad (A4)$$

For a ferrite medium biased by a dc magnetic field along an arbitrary direction, the four eigenmodes for wave propagation are, in general, nondegenerate [1]. Instead of using (4), the longitudinal wave number $k_z$ can now be solved from the following quartic equation:

$$P_4 k_z^4 + P_3 k_z^3 + P_2 k_z^2 + P_1 k_z + P_o = 0 \quad (A5)$$

where the polynomial coefficients are given by

$$P_4 = \omega_o^2 - \omega^2 + (e_{nx}^2 + e_{ny}^2)\omega_o\omega_m \quad (A6)$$

$$P_3 = -2e_{nz}(e_{nx}k_x + e_{ny}k_y)\omega_o\omega_m \quad (A7)$$

$$P_2 = -2(k_o^2 - k_x^2 - k_y^2)(\omega_o^2 + \omega_o\omega_m - \omega^2)$$
$$- [k_o^2 - e_{nz}^2(k_o^2 - k_x^2 - k_y^2) + (e_{nx}k_x + e_{ny}k_y)^2]\omega_o\omega_m$$
$$- (e_{nx}^2 + e_{ny}^2)k_o^2\omega_m^2 \quad (A8)$$

$$P_1 = 2e_{nz}(e_{nx}k_x + e_{ny}k_y)\omega_m[k_o^2\omega_m + (k_o^2 - k_x^2 - k_y^2)\omega_o] \quad (A9)$$

$$\underline{\underline{\Gamma}}(z) = \begin{pmatrix} \zeta e_{Ax}\exp(ik_z z) & \zeta e_{Ax}\exp(-ik_z z) & \zeta e_{Bx}\exp(ik_z z) & \zeta e_{Bx}\exp(-ik_z z) \\ \zeta e_{Ay}\exp(ik_z z) & \zeta e_{Ay}\exp(-ik_z z) & \zeta e_{By}\exp(ik_z z) & \zeta e_{By}\exp(-ik_z z) \\ e_{Bx}\exp(ik_z z) & -e_{Bx}\exp(-ik_z z) & -e_{Ax}\exp(ik_z z) & e_{Ax}\exp(-ik_z z) \\ e_{By}\exp(ik_z z) & -e_{By}\exp(-ik_z z) & -e_{Ay}\exp(ik_z z) & e_{Ay}\exp(-ik_z z) \end{pmatrix} \quad (A3)$$

$$P_o = \left(k_o^2 - k_x^2 - k_y^2\right) \Bigg\{ \left(k_o^2 - k_x^2 - k_y^2\right)\left(\omega_o^2 + \omega_o\omega_m - \omega^2\right)$$
$$+ \left[k_o^2 + (e_{nx}k_x + e_{ny}k_y)^2\right]\omega_o\omega_m$$
$$+ k_o^2\omega_m^2 \Bigg\} + \left(e_{nx}k_x + e_{ny}k_y\right)^2 k_o^2\omega_m^2.$$
$$(A10)$$

Here, $\underline{e}_n = (e_{nx}\ e_{ny}\ e_{nz})^T$ denotes the unit vector along the internal dc-bias field direction

$$k_o = \epsilon_f^{1/2}(\omega/c) \tag{A11}$$

$$\omega_m = 4\pi\gamma M_s \tag{A12}$$

$$\omega_o = \gamma H'_{\text{in}}. \tag{A13}$$

$\omega$ is the angular frequency, $\gamma$ is the gyromagnetic ratio, $c$ is the speed of light in vacuum, $\epsilon_f$ is the dielectric constant of the ferrite, $4\pi M_s$ is the saturation magnetization, and $H'_{\text{in}}$ is the effective internal bias magnetic field given by

$$H'_{\text{in}} = H_o - 4\pi M_s N_z + H_A - i\Delta H \text{ for an easy axis} \tag{A14a}$$

$$H'_{\text{in}} = \left[H_o(H_o + H_A)\right]^{1/2} - i\Delta H \text{ for an easy plane.} \tag{A14b}$$

Here, $H_o$ denotes the externally applied dc magnetic field and $\Delta H$ is the FMR linewidth. In (A14a), the easy axis occurs along the $z$-axis and the anisotropy field is denoted as $H_A$ [12, eq. (10)]. In (A14b), the easy plane lies on the $xy$-plane and the anisotropy field is $H_A$ [12, eq. (6)]. For practical applications, $H_o$ is applied along the easy-axis direction (the $z$-axis) or along a direction lying on the easy plane (the $xy$-plane). For the case of an easy axis, the demagnetizing field $4\pi M_s N_z$ needs to be subtracted from the total field, as expressed in (A14a). Here, $N_z$ denotes the axial demagnetizing factor, which may be estimated from a static calculation [7]. For cubic ferrites (e.g., garnets), the anisotropy field is small, and the total internal effective field, $H'_{\text{in}}$ is given by (A14a) assuming $H_A$ is negligible. Magnetic loss is accounted for by the term $-i\Delta H$ in (A14a) and (A14b), and dielectric loss can be included by using the following complex dielectric constant:

$$\epsilon_f \to \epsilon_f(1 + i\tan\delta_f). \tag{A15}$$

In (A15), $\tan\delta_f$ denotes the dielectric loss tangent of the ferrite material.

After $k_z$'s are solved from (A5), denoted as $k_{\alpha z}$, $\alpha = 1, 2, 3, 4$, the magnetic permeability $\mu_\alpha$ can be calculated from (4) as

$$\mu_\alpha = \left(k_x^2 + k_y^2 + k_{\alpha z}^2\right)/k_o^2. \tag{A16}$$

The associated electromagnetic fields are, therefore,

$$\underline{h}_\alpha = \underline{\underline{U}}\,\underline{h}_{\alpha'} \tag{A17}$$

$$\underline{e}_\alpha = \underline{\underline{U}}\,\underline{e}_{\alpha'} \tag{A18}$$

$$\underline{b}_\alpha = \underline{\underline{U}}\,\underline{b}_{\alpha'} \tag{A19}$$

where the primed fields are those expressed in a coordinate frame whose $z$-axis coincides with the internal dc-bias field direction [1]

$$h'_{\alpha x} = (i\omega/\gamma)\left(1 - \mu_\alpha\hat{e}_{\alpha1}^2\right) + H'_{\text{in}}\mu_\alpha\hat{e}_{\alpha1}\hat{e}_{\alpha2} \tag{A20}$$

$$h'_{\alpha y} = (-i\omega/\gamma)\mu_\alpha\hat{e}_{\alpha1}\hat{e}_{\alpha2} - H'_{\text{in}}\left(1 - \mu_\alpha\hat{e}_{\alpha2}^2\right)$$
$$- 4\pi M_s\left[1 + \mu_\alpha\hat{e}_{\alpha3}^2/(1 - \mu_\alpha)\right] \tag{A21}$$

$$h'_{\alpha z} = \hat{e}_{\alpha3}\mu_\alpha\left\{(-i\omega/\gamma)\hat{e}_{\alpha1} + \left[H'_{\text{in}} + 4\pi M_s/(1 - \mu_\alpha)\right]\hat{e}_{\alpha2}\right\} \tag{A22}$$

$$e'_{\alpha x} = -\zeta_\alpha\hat{e}_{\alpha3}\left[H'_{\text{in}} + 4\pi M_s(1 - \mu_\alpha\hat{e}_{\alpha1}^2)/(1 - \mu_\alpha)\right] \tag{A23}$$

$$e'_{\alpha y} = \zeta_\alpha\hat{e}_{\alpha3}\left[(-i\omega/\gamma) + 4\pi M_s\mu_\alpha\hat{e}_{\alpha1}\hat{e}_{\alpha2}/(1 - \mu_\alpha)\right] \tag{A24}$$

$$e'_{\alpha z} = \zeta_\alpha\Big\{H'_{\text{in}}\hat{e}_{\alpha1} + (i\omega/\gamma)\hat{e}_{\alpha2} + 4\pi M_s\hat{e}_{\alpha1}$$
$$\cdot \left[1 + \mu_\alpha\hat{e}_{\alpha3}^2/(1 - \mu_\alpha)\right]\Big\} \tag{A25}$$

$$b'_{\alpha x} = h'_{\alpha x} + (-i\omega/\gamma)(1 - \mu_\alpha) + 4\pi M_s\mu_\alpha\hat{e}_{\alpha1}\hat{e}_{\alpha2} \tag{A26}$$

$$b'_{\alpha y} = h'_{\alpha y} + H'_{\text{in}}(1 - \mu_\alpha) + 4\pi M_s\left(1 - \mu_\alpha\hat{e}_{\alpha1}^2\right) \tag{A27}$$

$$b'_{\alpha z} = h'_{\alpha z}. \tag{A28}$$

Here, $\underline{\hat{e}}_\alpha = (\hat{e}_{\alpha1}\ \hat{e}_{\alpha2}\ \hat{e}_{\alpha3})^T$ denotes the unit vector along the wave propagation direction $\underline{k}_\alpha = (k_x\ k_y\ k_{\alpha z})^T$, and $\zeta_\alpha = (\mu_\alpha/\epsilon_f)^{1/2}$ is the wave impedance. We note that for each mode $\alpha$, the three vectors $\underline{e}_\alpha$, $\underline{b}_\alpha$, and $\underline{k}_\alpha$ are mutually perpendicular to each other, as dictated by Maxwell equations. Also, $\underline{e}_\alpha$ is perpendicular to $\underline{h}_\alpha$, as can be readily verified. In (A17)–(A19), the coordinate transformation matrix $\underline{\underline{U}}$ is given by (A29), shown at the top of the following page, and $\Theta$ and $\Phi$ denote the polar and azimuthal angles along the internal bias field direction. That is, $\underline{e}_n = (\sin\Theta\cos\Phi, \sin\Theta\sin\Phi, \cos\Theta)^T$. Therefore, when $\underline{e}_\alpha$, $\underline{h}_\alpha$, and $\underline{k}_\alpha$, $\alpha = 1, 2, 3, 4$, are known from (A5), and from (A17)–(A29), the $\Gamma$-matrix of the ferrite layer can then be calculated using (2). The $T$-matrix can be calculated from the $\Gamma$-matrix by using (1).

## REFERENCES

[1] B. Lax and K. J. Button, *Microwave Ferrites and Ferrimagnetics.* New York: McGraw-Hill, 1962.
[2] N. Alexópoulos, "Integrated-circuit structures on anisotropic substrates," *IEEE Trans. Microwave Theory Tech.*, vol. MTT-33, pp. 847–881, Oct. 1985.
[3] T. Q. Ho and B. Becker, "Frequency-dependent characteristics of shielded broadside coupled microstrip lines on anisotropic substrates," *IEEE Trans. Microwave Theory Tech.*, vol. 39, pp. 1021–1025, June 1991.
[4] G. W. Hanson, "A numerical formulation of dyadic Green's functions for planar bianisotropic media with application to printed transmission lines," *IEEE Trans. Microwave Theory Tech.*, vol. 44, pp. 144–151, Jan. 1996.
[5] M. R. Rosa, M. L. Albuquerque, A. G. D'Assumcio, R. G. Maia, and A. J. Giarola, "Full wave analysis of microstrip lines on ferrite and anisotropic dielectric substrate," *IEEE Trans. Magn.*, vol. 25, pp. 2944–2946, July 1989.
[6] E. L.-B. El-Sharawy and R. W. Jackson, "Coplanar waveguide and slot line on magnetic substrates: Analysis and experiment," *IEEE Trans. Microwave Theory Tech.*, vol. 36, pp. 1071–1079, June 1988.

$$\underline{\underline{U}} = \begin{pmatrix} 1 - (1 - \cos\Theta)\cos^2\Phi & -(1 - \cos\Theta)\sin\Phi\cos\Phi & -\sin\Theta\cos\Phi \\ -(1 - \cos\Theta)\sin\Phi\cos\Phi & 1 - (1 - \cos\Theta)\sin^2\Phi & -\sin\Theta\sin\Phi \\ \sin\Theta\cos\Phi & \sin\Theta\sin\Phi & \cos\Theta \end{pmatrix} \tag{A29}$$

[7] H. How, "Magnetic microwave devices," in *Encyclopedia of Electrical and Electronics Engineering*, J. G. Webster, Ed. New York: Wiley, 1999, vol. 12, pp. 31–45.

[8] H. How, P. Shi, C. Vittoria, E. Hokenson, M. H. Champion, L. C. Kempel, and K. D. Trott, "Steerable phased array antennas using single-crystal YIG phase shifters—Theory and experiments," *IEEE Trans. Microwave Theory Tech.*, vol. 48, pp. 1544–1549, Sept. 2000.

[9] D. M. Pozar, "Radiation and scattering characteristics of microstrip antennas on normally biased ferrite substrates," *IEEE Trans. Antennas Propagat.*, vol. 30, pp. 1084–1092, Sept. 1992.

[10] H. How, S. A. Oliver, S. W. McKnight, P. M. Zavracky, N. E. McGruer, and C. Vittoria, "Theory and experiment of thin-film junction circulator," *IEEE Trans. Microwave Theory Tech.*, vol. 46, pp. 1645–1653, Nov. 1998.

[11] W. H. Von Aulock, Ed., *Handbook of Microwave Ferrite Materials*. New York: Academic, 1965.

[12] H. How, X. Zuo, and C. Vittoria, "Electromagnetic wave propagation involving a magnetic easy plane," *IEEE Trans. Microwave Theory Tech.*, submitted for publication.

[13] N. Zeina, H. How, and C. Vittoria, "Self-biasing circulators operating at $K_a$-band utilizing M-type hexagonal ferrites," *IEEE Trans. Magn.*, vol. 28, pp. 3219–3221, Sept. 1992.

[14] A. Sommerfeld, *Partial Differential Equations*. New York: Academic, 1962.

[15] H. How, W. Tian, and C. Vittoria, "AC Hall effect in multilayered semiconductors," *J. Lightwave Technol.*, vol. 15, pp. 1006–1011, June 1997.

[16] H. How and C. Vittoria, "Microstrip antennas," in *Encyclopedia of Electrical and Electronics Engineering*, J. G. Webster, Ed. New York: Wiley, 2000, Suppl. I, pp. 349–366.

[17] H. How, L. C. Kempel, K. D. Trott, and C. Vittoria, "Green's function calculation on circular microstrip patch antennas," *IEEE Trans. Antennas Propagat.*, vol. 49, pp. 393–401, Mar. 2001.

[18] M. Hashimoto, "A rigorous solution for dispersive microstrip," *IEEE Trans. Microwave Theory Tech.*, vol. MTT-33, pp. 1131–1137, Nov. 1985.

[19] G. E. Forsythe, M. A. Malcolm, and C. B. Moler, *Computer Methods for Mathematical Computations*. Englewood Cliffs, NJ: Prentice-Hall, 1977.

**Hoton How**, photograph and biography not available at time of publication.

**Xu Zuo**, photograph and biography not available at time of publication.

**Elwood Hokanson**, photograph and biography not available at time of publication.

**Leo C. Kempel** (S'86–M'95–SM'99) was born in Akron, OH, in October 1965. He received the B.S.E.E. degree from the University of Cincinnati, Cincinnati, OH, in 1989, and the M.S.E.E. and Ph.D. degrees from The University of Michigan at Ann Arbor, in 1990 and 1994, respectively.

He participated in the University of Cincinnati's cooperative education program at General Dynamics/Fort Worth Division. After a brief Post-Doctoral appointment at The University of Michigan at Ann Arbor, he joined the Mission Research Corporation in 1994 as a Senior Research Engineer. He led several projects involving the design of conformal antennas, computational electromagnetics, scattering analysis, and high-power/ultra-wide-band microwaves. In 1998, he joined Michigan State University, East Lansing, as an Assistant Professor, where he currently conducts research in computational electromagnetics, teaches undergraduate and graduate courses in electromagnetics, and supervises the research of several M.S. and Ph.D. students. He co-authored *The Finite Element Method for Electromagnetics: Antennas, Microwave Circuits, and Scattering Applications* (Piscataway, NJ: IEEE Press, 1998). He is a reviewer for *JEWA* and *Radio Science*.

Dr. Kempel is a member of Tau Beta Pi, Eta Kappa Nu, and Commission B of the International Scientific Radio Union (URSI). He served as the Chapter IV vice-chair for the Southeast Michigan Chapter of the IEEE, as well as the technical chairperson for the 2001 ACES Conference. He has organized several sessions at recent URSI and ACES meetings. He is a reviewer for several IEEE publications.

**Carmine Vittoria** (S'62–M'63–SM'83–F'90), photograph and biography not available at time of publication.

# UNITED STATES PATENT AND TRADEMARK OFFICE

COMMISSIONER FOR PATENTS
UNITED STATES PATENT AND TRADEMARK OFFICE
WASHINGTON, D.C. 20231
www.uspto.gov

| APPLICATION NUMBER | FILING DATE | GRP ART UNIT | FIL FEE REC'D | ATTY.DOCKET.NO | DRAWINGS | TOT CLAIMS | IND CLAIMS |
|---|---|---|---|---|---|---|---|
| 09/774,419 | 02/01/2001 | 2816 | 355 | | 2 | 14 | 2 |

**CONFIRMATION NO. 3844**

**FILING RECEIPT**

*OC000000006052740*

Hoton How
262 Clifton Street
Belmont, MA 02478

Date Mailed: 05/08/2001

Receipt is acknowledged of this nonprovisional Patent Application. It will be considered in its order and you will be notified as to the results of the examination. Be sure to provide the U.S. APPLICATION NUMBER, FILING DATE, NAME OF APPLICANT, and TITLE OF INVENTION when inquiring about this application. Fees transmitted by check or draft are subject to collection. Please verify the accuracy of the data presented on this receipt. If an error is noted on this Filing Receipt, please write to the Office of Initial Patent Examination's Customer Service Center. Please provide a copy of this Filing Receipt with the changes noted thereon. If you received a "Notice to File Missing Parts" for this application, please submit any corrections to this Filing Receipt with your reply to the Notice. When the USPTO processes the reply to the Notice, the USPTO will generate another Filing Receipt incorporating the requested corrections (if appropriate).

**Applicant(s)**

Hoton How, Belmont, MA;
Carmine Vittoria, Boston, MA;

**Domestic Priority data as claimed by applicant**

**Foreign Applications**

**If Required, Foreign Filing License Granted 05/08/2001**

**Projected Publication Date: 08/01/2002**

**Non-Publication Request: No**

**Early Publication Request: No**

** SMALL ENTITY **

**Title**

Electronically configurable microwave reflector

**Preliminary Class**

327

TITLE:      ELECTRONICALLY CONFIGURABLE
MICROWAVE REFLECTOR

## CROSS-REFERENCE TO RELATED APPLICATIONS

5

Not Applicable

## BACKGROUND — FIELD OF INVENTION

10        This invention is directed to a method and a device for obtaining electronically configurable microwave reflector. As a direct application, the reflection beam can be controlled and manipulated via electronically tuning or tailoring the local electromagnetic parameters, and hence the surface impedance, of the reflector, performing the functions of beam steering, forming, and nulling, etc..

15

## BACKGROUND — DESCRIPTION OF PRIOR ART

Microwave and millimeter-wave (MMW) devices and systems are becoming
20  increasingly important today for both defense and commercial applications. For example, in the collision avoidance industries, low-profile antennas are needed providing electronically steerable radiations to detect and identify obstacles and protrusions in front of a moving vehicle. Upon navigation the receiver antennas need to follow and trace the motion of GPS (Global Positioning Systems) satellites so as to continuously monitor and
25  report their positions. Also, there is a need to create radiation nulls along certain spatial directions for an antenna transmitter/receiver to warrant secure and covert communications. Other applications can be found in target searching/tracking radars, satellite communication systems, and TV program broadcasting antennas installed with a civilian jet carrier.

30

In a phased array system it is possible to include frequency-agile materials (varactors, ferroelectrics, and ferrites) to tune and adjust the phase and amplitude of each

individual element so as to compose and tailor the overall radiation into a desirable pattern. However, beam forming in this manner is costly; depending on the speed, frequency, and angle of steering, each phase-shifting element can cost as much as $1,000, and in a system containing 10,000 elements, the cost of the antenna array system can be

5 formidable. Power dissipation is another consideration, since amplifiers are used following each of the phase shifting processes to compensate signal propagation loss, or insertion loss. To avoid overheating, water cooling is, therefore, often required in a large phased array system.

10 A radiation beam can also be steered via mechanical means, as commonly observed for a traffic radar installed at the airports. However, steering in this manner is slow, suffering from potential mechanical breakdowns. To incorporate free rotation, the antenna take up considerable space and the shape of the antenna is not conformal. As such, it is unlikely to apply a mechanically rotating radar in a body moving at high speed.

15

A reflect-array antenna operates in the same manner as an optical grating device: The reflected beam is constructed coherently from each of the array elements according to its reflection phase and electric path [Berry, D.G., et al, IEEE Transaction Antennas and Propagation, vol.11, pp.645-651, 1963]. Therefore, by adjusting the phase and/or electric

20 path of the reflecting elements the overall beam construction can be controlled and manipulated, not only in its reflection direction, but also in its geometric shape, for example, beam width, side-lobe locations, and nulling directions.

In this invention specific reflect-array antennas are disclosed, electronically

25 configuring the elements for desired electromagnetic properties thereby providing beam-steering/beam-forming/beam-nulling capabilities. No amplifier is required and hence the problem of power dissipation is minimized. The reflector has a low profile containing no parts for mechanical rotation. The response time is fast and its fabrication is inexpensive.

30 Accordingly, it is an objective of the invention to address one or more of the foregoing disadvantages or drawbacks of the prior art, and to provide such improved method and device to obtain microwave beam-steering/beam-forming/beam-nulling

capabilities, permitting fast response with economy without requiring the use of mechanical parts for rotation and amplifiers for signal propagation-loss compensation.

Other objects will be apparent to one of ordinary skill, in light of the following
5   disclosure, including the claims.


## SUMMARY

10      In one aspect, the invention discloses a method and a device for microwave beam-steering/beam-forming/beam-nulling using a reflector whose electromagnetic parameters can be locally tuned or varied via electronic means. As a consequence, the reflection beam is constructed as superposition from all of the points, or elements, on the reflector surface whose phases and amplitudes presume pre-determined values. The overall shape of the
15   reflection beam can thus be composed into a desirable pattern.

In another aspect, the invention discloses a method and a device capable of locally changing the electromagnetic properties of a microwave reflector surface. The electric bias circuit, whose dimension compares much smaller than the wavelength of radiation, is
20   embedded in the ground plane. A frequency-agile layer, for example, a ferroelectric layer, is placed in close proximity to the bias circuit so that the dielectric constant of the layer can be locally adjusted via the bias circuit. As such, the bias circuit is invisible to the incident  microwave signal, and the ground plane plus the ferroelectric layer reflect the incident signal with locally varying surface impedance.
25

In another aspect, the invention discloses a method and a device capable of supplying additional inductance to a microwave reflector surface achieving optimal performance. For each surface element, device response may be simulated using a RCL circuit. For optimal performance the resonance frequency of the RCL circuit is devised
30   close to the frequency of application.  As such, the local surface impedance of the reflector shows a critical dependence on the bias voltage, resulting in fast phase tuning and rapid steering of the reflection beam. Inductance can be added to the system by depositing

-4-

isolated metal spots or patches on the reflector surface, although the bias circuit itself, which is electrically isolated from the ground plane, is effective in supplying inductance. Alternative, ferrite components (particle composites and/or multilayers, etc.) may be used as the inductive elements.

5

## BRIEF DESCRIPTION OF THE DRAWINGS

For a more complete understanding of the nature and objectives of the present
10 invention, reference is to be made to the following detailed description and accompanying drawings, which, though not to scale, illustrate the principles of the invention, and in which

FIG.1 shows one example of a reflector surface viewed from behind whose surface
15 impedance can be locally changed via electronic means. Four bias-circuits are shown embedded in the ground plane showing electric isolation. The bias-circuits are connected to four bias voltages which can be adjusted independently. A frequency-agile material is placed on top of the ground plane whose dielectric constant can be locally varied via the bias circuits.

20

FIG.2 shows the front view of the same example of FIG.1. In FIG.2 metal patches, in the form of discs, are deposited on the top surface of the frequency-agile material, providing additional inductance to the reflector surface to achieve optimal performance.

25

## DETAILED DESCRIPTION

### REFERENCE NUMERALS IN DRAWINGS

| 001 | Reflector Device |
| 30 100 | Ground Plane |
| 101, 102, 103, 104 | Bias Circuit for 4 Surface Elements |
| 200 | Frequency-Agile Material (Slab) |

| 311,312, 313, 314, 315, 316, 317, 318, 319 | Metal Patch (on Surface Element 1) |
| 321, 322, 323, 324, 325, 326, 327, 328, 329 | Metal Patch (on Surface Element 2) |
| 331, 332, 333, 334, 335, 336, 337, 338, 339 | Metal Patch (on Surface Element 3) |
| 341, 342, 343, 344, 345, 346, 347, 348, 349 | Metal Patch (on Surface Element 4) |

5

## PREFERRED EMBODIMENT: BACK VIEW — FIG.1

10    FIG.1 shows an example of the preferred embodiment of the invention viewed from behind the reflector device **001**. In FIG.1 ground plane **100** is deployed on the back side of a frequency-agile material **200** whose dielectric constant, or electric permittivity, can be varied by applying a bias electric field. To be explicit, the frequency-agile material **200** can be a piece of ferroelectric slab, or in combination with other dielectric/magnetic layers (including air). Slot-windows are cut on the ground plane **100** within which electric

15    bias circuits **101**, **102**, **103**, **104** are allocated showing electric isolation from the ground plane **100**. That is, electric bias circuit **101** is biased by a voltage $V_1$ in reference to the ground plane **100**, electric bias circuit **102** is biased by a voltage $V_2$ in reference to the ground plane **100**, electric bias circuit **103** is biased by a voltage $V_3$ in reference to the ground plane **100**, and electric bias circuit **104** is biased by a voltage $V_4$ in reference to

20    the ground plane **100**. The bias field, or electric flux lines, is generated in the vicinity of the window-slot regions separating the bias circuits **101**, **102**, **103**, **104** from the ground plane **100**, leaking into the frequency-agile material **200**, thereby influencing or affecting the dielectric constant, or electric permittivity, there.

25    Thus, the reflector device **001** of FIG.1 is divided in four regions, called surface elements, whose effective dielectric constants, or electric permittivities, are determined or controlled by the bias voltage $V_1$, $V_2$, $V_3$, and $V_4$. Although 4 surface elements are illustrated in FIG.1, the surface elements can take any number, depending on the need of the device application: the narrower the reflection beam width, the

30    larger the number of surface elements required. The bias circuit **101**, **102**, **103**, **104** can assume other geometries, not necessarily to be that shown in FIG.1. For example, the

spiral geometry is also considered to be effective. By using the printing-circuit techniques, the ground plane **100** and the bias circuits **101, 102, 103, 104** can be readily fabricated on the back side of the frequency-agile material **200** in a cost effective manner.

5

The fine detail of the bias circuits **101, 102, 103, 104** is invisible to the microwave signals incident from the front side of the reflector device **001**, assuming the width of the slot windows cut on the ground plane **100** to be much smaller than the wavelength of the radiation. That is, meshes on the ground plane **100** will not be seen

10 by the radiation if the dimension of the mesh holes is small compared to the wavelength. Thus, the incident wave is reflected by the ground plane **100** experiencing locally different dielectric constants, or electric permittivities, impressed on the adjacent dielectric matching layer, say, the frequency-agile material **200**, resulting in steering/forming/nulling of the reflection beam in a desired manner.

15

## PREFERRED EMBODIMENT: FRONT VIEW — FIG.2

FIG.2 shows the front view of the same reflector device **001** shown in FIG.1. In

20 FIG.2 metal patches **311, 312, 313, 314, 315, 316, 317, 318, 319** are deposited on the front side of surface element 1 of the frequency-agile material **200,** metal patches **321, 322, 323, 324, 325, 326, 327, 328, 329** are deposited on the front side of surface element 2 of the frequency-agile material **200,** metal patches **331, 332, 333, 334, 335, 336, 337, 338, 339** are deposited on the front side of surface element 3 of the

25 frequency-agile material **200,** and metal patches **341, 342, 343, 344, 345, 346, 347, 348, 349** are deposited on the front side of surface element 4 of the frequency-agile material **200**. These metal patches can also be fabricated using printing circuit techniques. They may assume different geometries, so long as their dimension is much smaller than the wavelength and they are electrically isolated from each other.

30

To optimally operate the reflector device **001** we expect that the surface

impedances of the four surface elements shown in FIGs.1 and 2 depend critically on the bias voltages $V_1$, $V_2$, $V_3$, and $V_4$. That is, when the electromagnetic response from each of the surface elements is modeled by a RCL circuit, we would hope the resonant frequency of the circuits, $\omega_r = (LC)^{-1}$, to be close to the applied frequency, $\omega_o$, so that

5   a slight change in C, or in the bias voltage, results in a sensitive change in the circuit impedance, $Z = (R^{-1} + j\omega C + 1/j\omega L)^{-1}$. This requires (additional) inductance to be incorporated into the surface elements, as prescribed by the application frequency $\omega_o$. For this purpose metal patches, **311, 312, 313, ···, 347, 348, 349** are thus introduced in the surface elements 1 to 4 shown in FIG.2. We note that it is the surface impedance

10  that is responsible for the change in the reflection phase for each of the surface elements.


Additional inductance is introduced via metal patches **311, 312, 313, ···, 347, 348, 349** due to the added eddy currents [H. How, et al, IEEE Antennas and

15  Propagation Symposium Digest, pp. 1208, May 1990]. We note that inductance is also added to the surface elements by the four bias circuits **101, 102, 103, 104**, shown in FIG.1. The effective permittivity and permeability of the surface elements are denoted as $(\epsilon_1, \mu_1)$, $(\epsilon_2, \mu_2)$, $(\epsilon_3, \mu_3)$, and $(\epsilon_4, \mu_4)$, for the four surface elements 1, 2, 3, 4, respectively. Although in FIG.2 we have assumed equal amount of inductance, or the

20  same number of identical metal patches, for each of the four surface elements, this is not necessary. For example, to synthesize a large diffraction angle, $\mu_1$, $\mu_2$, $\mu_3$, and $\mu_4$ assume very different values so as to generate high-order grating effects. In FIG.2 we have included isolated metal patches, **311, 312, 313, ···, 347, 348, 349**, to furnish inductance. Alternatively, ferrite components can be used for the same purpose. For

25  example, the frequency-agile material **200** may contain ferrite particles or multiple dielectric/magnetic layers as metamaterials.



## CONCLUSIONS

30

The present invention discloses a method that allows the local surface

impedance of a microwave reflector to vary with the impressed bias electric fields, enabling the overall reflection phase and amplitude to be composed in a desirable manner. The bias circuits are enclosed with the ground plane maintaining mutual electric isolation, and a frequency-agile material is used in contact with the ground

5   plane. Thus, by varying the bias voltages, the local dielectric constant of the frequency agile material is changed, resulting in changes in the local surface impedance. The bias circuits are invisible to the incident microwave signal, since their dimensions are much smaller than the wavelength of the radiation. Additional inductance can be included by introducing metal patches and/or ferrite particles in the reflector system.

10

The present invention discloses a device that a frequency-agile layer is deposited with a ground plane in which electric bias circuits are included maintaining electric isolation from the ground plane. By applying a bias voltage to the bias circuit in reference to the ground plane a local electric field is established so as to affect the

15   dielectric constant of the frequency-agile layer nearby. This results in changes in the local surface impedance of the reflector device. Thus, when a microwave signal is incident upon the reflector from the other side of the frequency-agile layer, it penetrates into the layer experiencing different phase changes at local sites, reflected by the ground plane, re-composing after transmission, performing beam forming, beam

20   steering, and beam nulling functions for overall reflection.

The scope of the invention should be determined by the appended claims and their legal equivalent, rather than by the examples given. It is also understood that the following claims are to cover all generic and specific features of the invention

25   described herein, and all statements of the scope of the invention which, as a matter of language, might be said to fall there between.

## CLAIMS

We claim:

5    1.    A method of locally varying and controlling the electromagnetic properties
          of a reflector device, comprising:
          incorporating a plural of electric bias circuits embedded in, and kept in
          electric isolation with, the ground plane of said reflector device;
          incorporating a frequency-agile material placed in close proximity to said
10        ground plane and said bias circuits whose dielectric constant can be changed
          via the local bias field impressed nearby,
          wherein by adjusting the bias voltages applied to said electric bias circuits in
          reference to said ground plane local surface impedance of said reflector
          device can be varied and controlled, resulting in reflection of the incident
15        electromagnetic signal in a pre-determined manner.

     2.    The method of claim 1 wherein electrically isolated metal spots or
          patches are introduced into said reflector device to locally control the
          amount of inductance to affect said local surface impedance.

20

     3.    The method of claim 1 wherein ferrite components are introduced into
          said reflector device to locally control the amount of inductance to
          affect said local surface impedance.

25   4.    The method of claim 2 wherein said metal spots or patches are
          much smaller in dimension than the wavelength of said incident
          electromagnetic signal.

     5.    The method of claim 1 wherein in accommodating said electric bias
30        circuits said ground plane is cut into slot windows with widths much
          smaller than the wavelength of said incident electromagnetic signal.

6.   The method of claim 1 wherein said local surface impedance is devised near resonance of an effective RCL circuit.

5

7.   The method of claim 1 wherein said frequency-agile material includes a ferroelectric layer.

8.   An electronically configurable reflector device capable of providing local adjustment of its surface impedance, comprising:

10

(A) a frequency-agile layer whose dielectric constant can be changed by applying a local electric bias field;

(B) a ground plane on one side of said frequency-agile layer with slot-cut windows of pre-determined geometries;

(C) a plural of electric bias circuits in the form of metal patches or metal

15

strips placed in said slot-cut windows of said ground plane maintaining mutual electric isolation,

wherein, by applying bias voltages to said bias circuits in reference to said ground plane with pre-determined magnitudes, an electromagnetic signal incident from the other side of said frequency-agile layer of said reflector

20

device opposing to said ground plane and said electric bias circuits is reflected by said ground plane, experiencing different local surface impedance of said reflector device, performing beam steering, beam forming, and/or beam nulling functions in a desirable manner.

25

9.   The electronically configurable reflector device of claim 8 wherein said slot-cut windows in said ground plane are much smaller in dimension than the wavelength of said electromagnetic signal.

10.   The electronically configurable reflector device of claim 8 wherein said

30

frequency-agile layer includes a ferroelectric component.

11. The electronically configurable reflector device of claim 8 wherein electrically isolated metal patches or spots are introduced with said frequency-agile layer contributing additional inductance to the performance of said reflector device.

5

12. The electronically configurable reflector device of claim 8 wherein ferrite components are introduced with said frequency-agile layer contributing additional inductance to the performance of said reflector device.

10

13. The electronically configurable reflector device of claim 8 wherein said reflector device assumes a planar geometry.

14. The electronically configurable reflector device of claim 8 wherein said reflector device assumes the geometry of a parabola.

15

# ELECTRONICALLY CONFIGURABLE
# MICROWAVE REFLECTOR

**Abstract** : Disclosed is a method and a device for obtaining local adjustment of the

5   surface impedance of a microwave reflector. The adjustment is accomplished via

electronic means. That is, the reflector is made of frequency-agile material whose

dielectric constant can be changed by applying a bias electric field. By inserting the

bias circuits within the ground plane maintaining mutual electric isolation, surface

impedance of the reflector device can thus been locally varied. Additional inductance is

10   added to the reflector system by introducing electrically isolated metal spots and/or

metal patches. The device operates near an inductor-capacitor resonance so that the

surface impedance varies sensitively with the bias voltages. The reflector assumes a low

profile whose fabrication is compatible with the printing-circuit techniques. It requires

no mechanical parts and hence it is operational at high speed. The reflector device

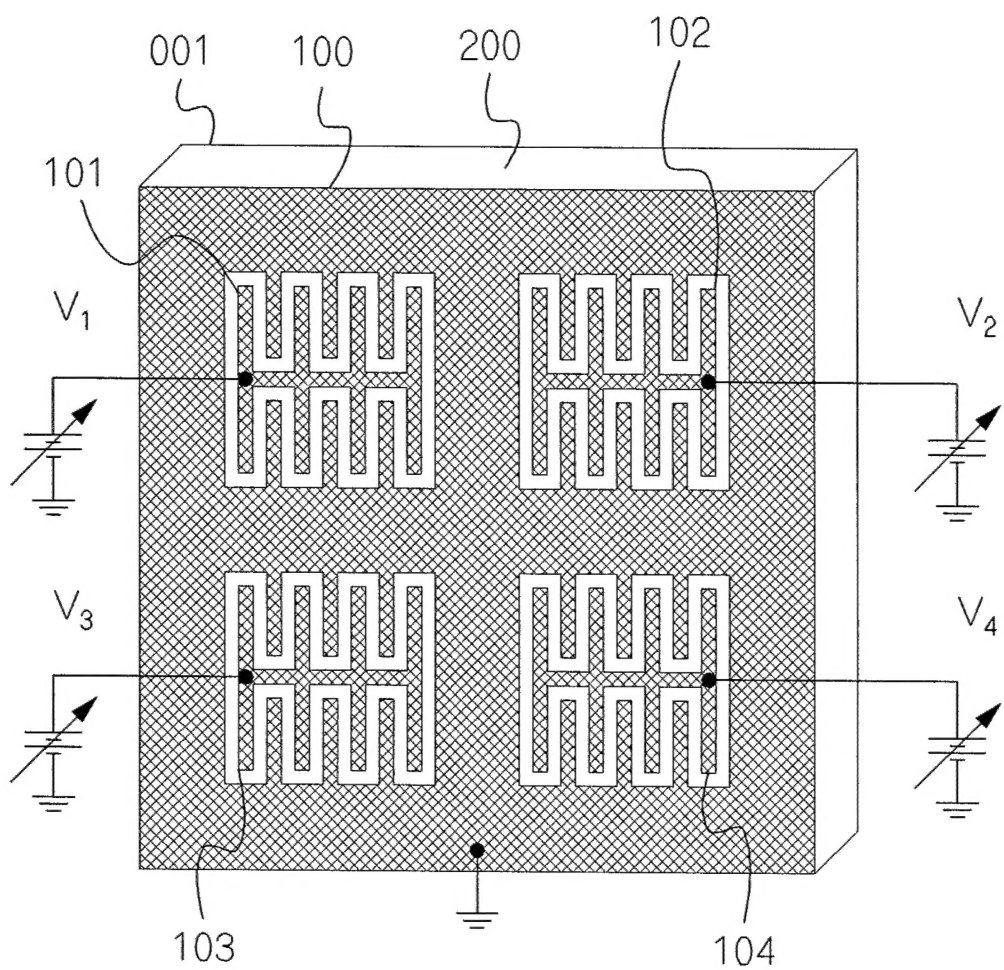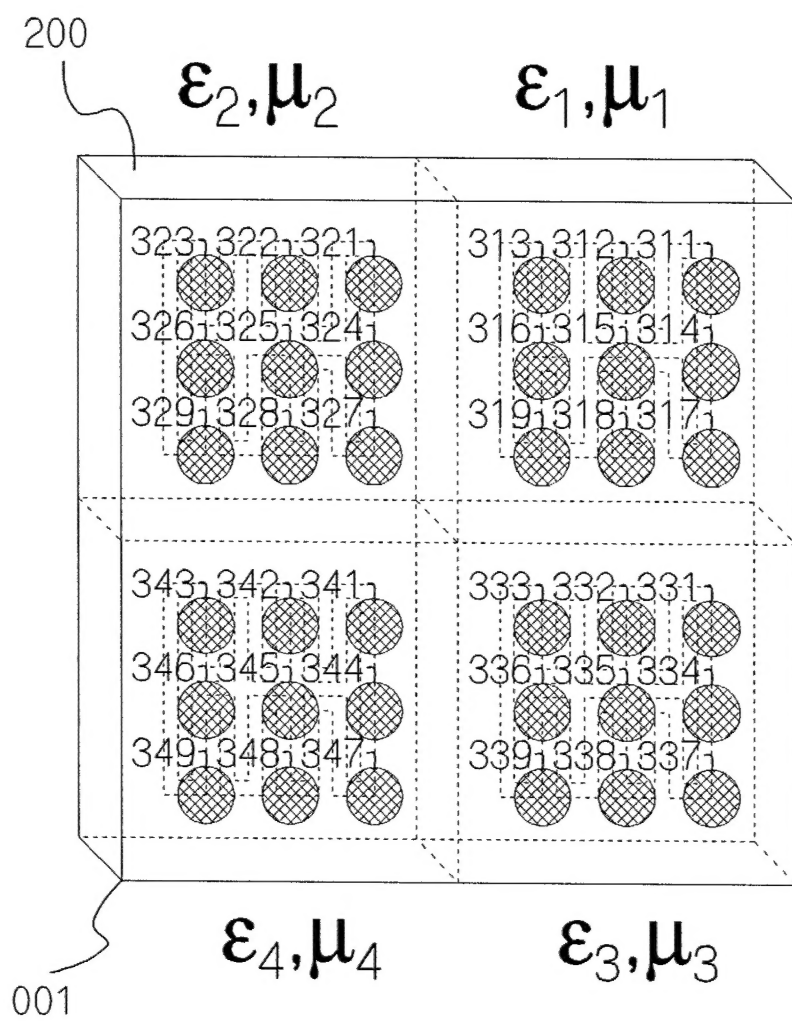15   performs the following functions: beam forming, beam steering, and beam nulling.

001  100  200  102

101

$V_1$

$V_3$

$V_2$

$V_4$

103  104

# FIG.1

FIG.2